UPPSALA
UNIVERSITET

Digital Comprehensive Summaries of Uppsala Dissertations from the Faculty of Science and Technology 1802

Avoiding ageing

Surface degradation of commercial electrode materials in lithium-ion batteries

ERIK BJÖRKLUND

ACTA
UNIVERSITATIS
UPSALIENSIS
UPPSALA
2019

ISSN 1651-6214
ISBN 978-91-513-0639-1
urn:nbn:se:uu:diva-381548

Dissertation presented at Uppsala University to be publicly examined in Room 4001, Ångströmlaboratoriet, Lägerhyddsvägen 1, Uppsala, Wednesday, 5 June 2019 at 09:15 for the degree of Doctor of Philosophy. The examination will be conducted in English. Faculty examiner: Prof. dr. Frank Renner (Hasselt University).

Abstract
Björklund, E. 2019. Avoiding ageing. Surface degradation of commercial electrode materials in lithium-ion batteries. *Digital Comprehensive Summaries of Uppsala Dissertations from the Faculty of Science and Technology* 1802. 72 pp. Uppsala: Acta Universitatis Upsaliensis. ISBN 978-91-513-0639-1.

The battery market today expands rapidly, not least for electric vehicles. But to compete against the combustion engine, the cost of batteries must be reduced. After years of usage, the batteries degrade and need to be exchanged, increasing the cost over the vehicle lifecycle. This can be mitigated by tailoring the usage conditions and the battery materials. Understanding and avoiding ageing can be key to a more sustainable transport system. This thesis contains studies on degradation processes in Li-ion batteries utilizing the $LiNi_xMn_yCo_zO_2$ (NMC) cathode material, and suggests strategies for the improvement of battery life time.

When cycling different negative electrodes – including graphite, lithium foil and lithium titanium oxide (LTO) – against NMC electrodes, only minor capacity fading was observed in the NMC-LTO and NMC-graphite cells, in contrast to the NMC-Li-metal cells. The capacity fading for Li-metal cells was determined to be caused by degradation products formed at the lithium foil which thereafter diffused to the NMC electrode, leading to a higher resistance. Commercial NMC/$LiMn_2O_4$-graphite cells were also investigated after cycling in limited state of charge (SOC)-intervals. The cycle life was far longer in the low-SOC cell than in the high-SOC cell. Photoelectron spectroscopy revealed increased manganese dissolution in the high-SOC cell, likely causing a less stable solid electrolyte interphase layer on the negative electrode. This, in turn, limits the capacity. How temperature influence ageing in NMC-LTO was analysed in cells cycled at -10 °C, 30 °C and 55 °C. It was found that the initial side reactions at the LTO electrode limited the cell capacity, but that these also stabilized the NMC electrode. At 55 °C, excessive side reactions at LTO caused capacity fading due to loss of active lithium. At -10 °C, high cell resistance limited the capacity. Switching to a PC based electrolyte allowed stable low temperature cycling, although it was found that PC degraded and formed thick electrode surface layers. Also sulfolane-based electrolytes were investigated, showing thinner surface layers than the EC containing reference electrolyte at high potentials, thus indicating a more stable electrolyte system.

Keywords: Li-ion battery, Ageing, Photoelectron spectroscopy, Nickel Manganese Cobalt Oxide

Erik Björklund, Department of Chemistry - Ångström Laboratory, Structural Chemistry, Box 538, Uppsala University, SE-751 21 Uppsala, Sweden.

ISSN 1651-6214
ISBN 978-91-513-0639-1
urn:nbn:se:uu:diva-381548 (http://urn.kb.se/resolve?urn=urn:nbn:se:uu:diva-381548)

List of Papers

This thesis is based on the following papers, which are referred to in the text by their Roman numerals.

I **How the negative electrode influence interfacial and electrochemical properties of $LiNi_{0.33}Mn_{0.33}Co_{0.33}O_2$ cathodes in Li-ion batteries**
E. Björklund, D. Brandell, M. Hahlin, K. Edström, and R. Younesi
Journal of the Electrochemical Society, 164 (2017) A3054-A3059.

II **Temperature dependence of electrochemical degradation in $LiNi_{0.33}Mn_{0.33}Co_{0.33}O_2/Li_4Ti_5O_{12}$ cells**
E. Björklund, A. J. Naylor, W. Brant, D. Brandell, R. Younesi and K. Edström
Submitted manuscript.

III **Investigation of dimethyl carbonate and propylene carbonate mixtures for $LiNi_{0.6}Mn_{0.2}Co_{0.2}O_2$-$Li_4Ti_5O_{12}$ cells**
E. Björklund, M. Göttlinger, K. Edström, D. Brandell and R. Younesi
Submitted manuscript.

IV **Sulfolane based EC-free electrolytes in high voltage cells**
E. Björklund, M. Göttlinger, K. Edström, R. Younesi and D. Brandell
In manuscript.

V **Influence of state-of-charge in commercial $LiNi_{0.33}Mn_{0.33}Co_{0.33}O_2/LiMn_2O_4$-graphite cells analyzed by synchrotron-based photoelectron spectroscopy**
E. Björklund, E. Wikner, R. Younesi, D. Brandell and K. Edström
Journal of Energy Storage, 15 (2018) 172-180.

Reprints were made with permission from the respective publishers.

Comments on my contribution to the papers in this thesis:

I Planned most of the work, performed the electrochemical and spectroscopic measurements. Took part in the spectroscopic data analysis. Wrote the manuscript with co-authors.

II Planned most of the work, performed electrochemical and spectroscopic measurements including the data analysis. Wrote the manuscript while receiving input from the co-authors.

III Planned most of the work, performed some of the electrochemical and all of the spectroscopic measurements. Wrote the manuscript while receiving input from the co-authors.

IV Planned most of the work, performed electrochemical and spectroscopic measurements including the data analysis. Wrote the manuscript while receiving input from the co-authors.

V Planned most of the work, performed electrochemical and spectroscopic measurements including the data analysis (on cells that had already reached end-of-life). Wrote the manuscript while receiving input from the co-authors.

Disclaimer: Parts of this thesis are based on my licentiate thesis entitled "Insights into the surface chemistry of $LiNi_{0.33}Mn_{0.33}Co_{0.33}O_2$ in Li-ion cells" (Uppsala University, 2017).

Other published papers not included in this thesis:

I **LiTDI: A Highly Efficient Additive for Electrolyte Stabilization in Lithium-Ion Batteries**
C. Xu, S. Renault, M. Ebadi, Z. Wang, E. Björklund, D. Guyomard, D. Brandell, K. Edström, T. Gustafsson
Chem. Mater., 29 (2017) 2254-2263

Contents

Abbreviations

CMC	Carboxymethyl cellulose
DEC	Diethyl carbonate
DMC	Dimethyl carbonate
EC	Ethylene carbonate
EMC	Ethyl methyl carbonate
ESCA	Electron spectroscopy for chemical analysis
EXAFS	Extended x-ray absorption fine structure
HAXPES	Hard x-ray photoelectron spectroscopy
HOMO	Highest occupied molecular orbital
ICA	Incremental capacity analysis
LCO	Lithium cobalt oxide ($LiCoO_2$)
LFP	Lithium iron phosphate ($LiFePO_4$)
LIB	Lithium-ion battery
LiBOB	Lithium bis(oxalate)borate
LiTFSI	Lithium bis(trifluoromethane sulfonyl)imide
LMO	Lithium manganese oxide ($LiMn_2O_4$)
LSV	Linear sweep voltammetry
LTO	Lithium titanium oxide ($Li_4Ti_5O_{12}$)
LUMO	Lowest unoccupied molecular orbital
NMC	Lithium nickel manganese cobalt oxide ($LiNi_{0.33}Mn_{0.33}Co_{0.33}O_2$)
NMC (622)	Lithium nickel manganese cobalt oxide ($LiNi_{0.6}Mn_{0.2}Co_{0.2}O_2$)
NMP	N-methyl-2-pyrrolidone
OCV	Open circuit voltage
PC	Propylene carbonate
PES	Photoelectron spectroscopy
SEI	Solid electrolyte interphase
SBR	Styrene-butadiene rubber
SOC	State of charge
SOXPES	Soft x-ray photoelectron spectroscopy
SPE	Solid polymer electrolyte

R_{wp}	weighted profile R-factor
XANES	X-ray absorption near edge structure
XPS	X-ray photoelectron spectroscopy
XRD	X-ray diffraction

1. Introduction

1.1 Lithium-Ion Batteries

Lithium-ion batteries (LIBs) combine some of the most useful properties in a battery, including large capacity and large potential differences between the electrodes. The capacity of a cell refers to the amount of charge which is transported during charge or discharge, and the potential differences between the electrodes corresponds to the cell voltage. The combination of large cell voltage and large capacity gives a large energy content of the cell, i.e. the amount of useful work the cell can perform until the potential difference between the electrodes decreases to a value lower than what is useable. The size of the lithium ion is small, which allows construction of electrodes being able to store large amounts of energy in a small volume and with low mass; i.e., LIBs can achieve both a high volumetric and gravimetric energy density.[1] The small size of the lithium ion also allows the active electrode materials to react with the lithium ions without causing large internal stresses in the material, thereby avoiding material degradation. The possibility of rapid discharge processes of LIBs, delivering high currents, is another beneficial property.

LIBs generally consist of a positive electrode, a negative electrode, a separator and an electrolyte.[2] The role of the electrolyte is to transport the lithium ions between the electrodes without transporting electrons or undergoing undesired side-reactions. The separator is used to prevent contacts between the two electrodes in order to prevent internal short circuits.

During discharge of the battery, the positive electrode is reduced and the negative is oxidized as lithium ions leave the anode and intercalates into the cathode, whereas during charging these processes are reversed as the lithium ions move from the positive electrode towards the negative electrode; see Fig. 1. In a rechargeable battery, these processes should ideally be repeated for thousands of cycles. Unfortunately, unwanted side-reactions will take place simultaneously to the intercalation of lithium ions, thereby degrading the cell materials,[3] primarily the electrodes and electrolyte. The degradation of the cell materials will eventually lead to cell failure, and the cells in the device have to be replaced by new ones. In commercial applications, such as batteries for portable electronics, it is therefore important to prolong the cycle life in order to minimize the use of natural resources and the price for the customer. This become even more important in large-scale applications such as batteries for electric vehicles, which contain more material.

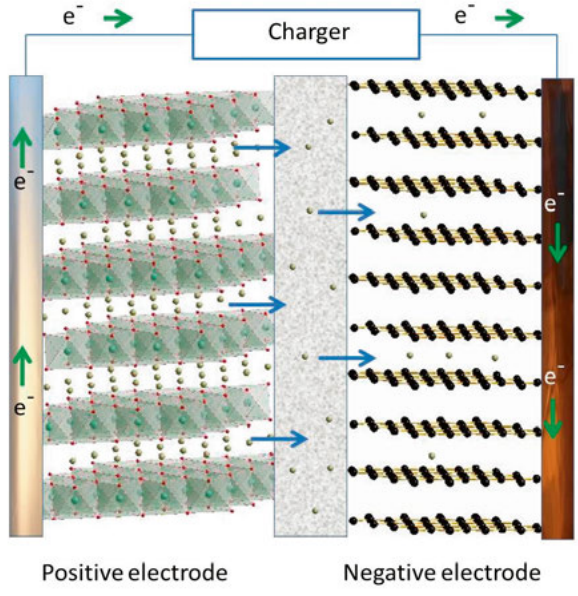

Figure 1. Schematic illustration of the charging process of a LIB.

1.2 Electrode Materials

1.2.1 Positive electrodes

The active material in the positive electrode should react reversibly with lithium ions at a high potential vs. Li/Li^+. Moreover, in order to achieve high reaction rates, the host material must possess fast lithium ion diffusion. The atomic structure is therefore important, where layered structures are common as the lithium ions can move between the layers in two dimensions comparatively easy. Several layered oxide materials have been commercialized, such as lithium cobalt oxide (LCO) and lithium nickel manganese cobalt oxide (NMC). Materials in which the lithium ions can only diffuse in one dimension have also shown commercial success, e.g. lithium iron phosphate (LFP).[4,5] In order to not be limited by its slow solid state diffusion, LFP electrodes often consist of nano-sized particles,[6,7,8] as compared to other electrode materials where the particle size can be about 10 µm.

In order to achieve a high gravimetric energy density, the active material in the positive electrode usually consists of lithium together with lighter p-block elements and first row d-block elements. These are all comparatively lightweight atoms, and the heavier d-block metals can undergo straight-forward redox reactions during lithium insertion and deinsertion.

Lithium manganese oxide (LMO) is another important material used in positive electrodes. It has a spinel structure allowing lithium ion diffusion

through diffusion pathways in three dimensions.[9] The diffusion pathways permit rapid transport of lithium ions which renders high rate capability. As LMO does not contain cobalt, it is generally considered more environmental friendly than LCO or NMC. LMO on the other hand experiences problem with manganese dissolution,[10] as manganese ions can dissolve from the electrode and deposit on the negative electrode. Also new phases might be created during cycling of LMO,[10] as well as loss of oxygen during delithiation, resulting in capacity losses.[11] A summary of specific capacities and operating potentials of various common electrode materials is illustrated in Fig. 2.

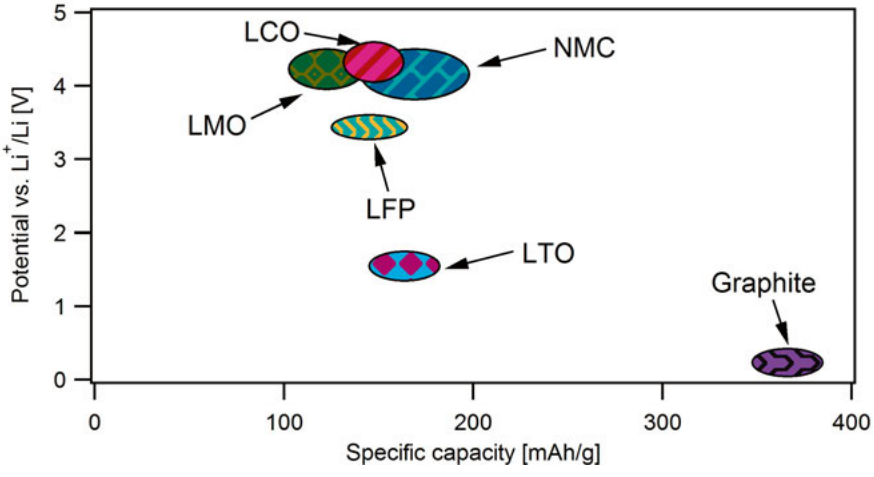

Figure 2. Approximate specific capacities and discharge potentials of common LIB electrode materials.

1.2.2 Negative electrodes

The negative electrode should operate at as low electrochemical potential as possible in order to maximize the potential difference between the electrodes. In commercial LIB cells, graphite is the most common negative electrode material. Graphite has a high specific capacity as compared to almost all commercial cathode materials, but not as high as some other investigated anode materials. Graphite is a crystalline layered structure where lithium ions can intercalate during charging. Graphite electrodes operate at a potential close to lithium metal,[12] which might lead to lithium plating on the electrode.[13] Also surface layer formation consisting of electrolyte degradation products will take place,[14] increasing the resistance in the cell and consuming lithium ions. The increased resistance hinders the Li-ion transport, leading to an increased potential during charging (or decreased potential during discharging), causing the cut-off potential to be reached before the electrodes are fully delithiated or lithiated and thereby decreasing the capacity and the cycle life. The surface

layer formation differs depending on surface imperfections, e.g. edges and defects can cause increased electrolyte decomposition, making the edge to basal plane ratio an important factor.[15]

Lithium metal is commonly used in battery cells, not least in academic research studies. It would also be an ideal material in commercial batteries if its safety could be improved.[16] The capacity of Li-metal is extremely high, about 3860 mAh/g (in the charged state).[17] Additionally, the potential is very low,[18] rendering cells with a high energy density. However, uneven deposition of lithium often occurs during the lithiation process, making the surface rough. Dendrites will form as a result, which eventually will penetrate the separator and short-circuit the battery after some cycles.[19] This can cause overheating and lead to what is known as a 'thermal runaway'.[20] This is the main cause forcing LIB producers to use other negative electrode materials. Similarly to graphite, the electrolyte will also degrade on Li-metal and form a surface layer on the electrode which increases the internal resistance and decreases the capacity.

LTO is yet another negative electrode material, where many of the problems associated with graphite or lithium metal are solved intrinsically. LTO operates at a significantly higher electrochemical potential where it is less thermodynamically favorable to form surface layers from electrolyte decomposition products, making it possible to cycle the electrode reversibly for an extensive number of cycles. The high lithiation/delithiation potential also makes it possible to use aluminum current collectors instead of copper, which is a cheaper and more light-weight material.[21] Additionally, the high operating potential as compared to lithium also makes the risk of lithium plating on the electrode minimal.[22] The LTO material has a comparably slow solid state mobility of lithium ions, but this problem can be mitigated by using LTO particles that are nano- sized instead of micro-sized, shortening the diffusion length and thus allowing cycling at high rates. In the delithiated state, LTO has a cubic spinel structure, allowing three-dimensional diffusion of Li-ions, which transforms into a rock salt structure in the lithiated state. The structural change during lithiation results in a very minor volume change, causing very small internal stresses. LTO thus undergoes little internal strain as compared to other electrode materials during delithiation and lithiation, which also contributes to long cycle life[23] as the material will not undergo structural degradation. However, its high operational potential is not exclusively beneficial, since it also directly decreases the energy density of the cell.[24] The capacity of LTO is also lower than that of graphite. Moreover, at higher potentials the electrolyte might react through other mechanisms and form gases. Due to these reasons, LTO is much less used than graphite in commercial batteries.

1.3 Electrolytes

The purpose of the electrolyte is to transport ions between the electrodes during battery cycling. An electrolyte should not have any electrical conduction in order to prevent internal short circuits. The electrolyte should also ideally not participate in any redox reaction where it is consumed, i.e. it should be chemically inert with the respect to the electrodes. There are many kinds of electrolytes depending on the device intended for the LIB: liquid electrolytes, solid polymer electrolytes (SPEs), gel polymer electrolytes, ionic liquids and ceramic electrolytes. Liquid electrolytes are most common due to their high conductivity of lithium ions and their ability to dissolve lithium salts. The electrolytes normally consist of a salt dissolved in an organic solvent, where the salt concentration to a large extent determines the conductivity. A low concentration would give a low conductivity because the electrolyte would have few charge carriers, whereas a too high concentration would increase the viscosity and thereby decreasing the mobility of the ions. Besides the salt concentration, the viscosity will also be influenced by the solvent molecules, making the choice of solvent an important factor to achieve a high conductivity. Furthermore, the solvent molecules will coordinate to the lithium ions, and the strength of this interaction will also affect how easily the lithium ions can be transported in the electrolyte. This interaction is generally estimated from the dielectric constant, where a high dielectric constant is a measure of how easily the salt will be disassociated in a solution.[25,26] If the dielectric constant is high, the coordination between the solvent and the lithium ion will be stronger.[27] A low dielectric constant will therefore instead lead to ion association and lower conductivity.[25]

Common solvents in LIBs are low-Mw carbonate-based hydrocarbons such as diethyl carbonate (DEC), dimethyl carbonate (DMC), ethyl methyl carbonate (EMC) and ethylene carbonate (EC).[28] The linear carbonates DMC, EMC, and DEC have low viscosity and decent stability, but low dielectric constants. EC on the other hand has a high viscosity and a melting point as high as 36 °C,[28] but has a high dielectric constant. It degrades fairly easy at low potentials, forming a polymeric film on the negative electrode. This film stabilizes graphite electrodes, which is why EC is a common co-solvent in commercial LIBs. A related solvent is propylene carbonate (PC). PC has many beneficial properties: high dielectric constant, high boiling point and low melting point. It will, however, be cointercalated into graphite during cycling, leading to exfoliation of this active anode material and is therefore avoided in cells containing graphite as the negative electrode material.

The most common salt in LIBs is $LiPF_6$, frequently used at a concentration of about 1 mol/dm^3, but other salts are also found, e.g. lithium bis(trifluoromethane sulfonyl)imide (LiTFSI), lithium bis(oxalate)borate (LiBOB) and lithium perchlorate ($LiClO_4$). $LiPF_6$ is beneficial since it dissolves easily in many solvents, contributes to decent ion conduction and forms a passivating

film on aluminum, which is normally used as current collector on the positive electrode – and thereby prevents it from corrosion. There are also some drawbacks associated with $LiPF_6$, not least salt degradation. The PF_6^- anion reacts with trace amounts of water and then form HF, which can react further with the solvent and the electrodes. LiTFSI, on the other hand, while also rendering a reasonably high ionic conductivity does not form a good passivating film on aluminum. This makes it difficult to utilize in a liquid electrolyte system when having aluminum as current collector.

To maximize the energy density, many novel positive electrode materials strive to operate at higher potentials, thereby increasing the potential difference in the cells. This increases the difficulty of finding electrolytes which are electrochemically stable and do not undergo redox reactions as the environment changes from strongly oxidizing (at the cathode) to strongly reducing (at the anode). It has been reported that by using a much higher salt concentration, the resistance towards redox reactions of the electrolyte is increased since the solvent molecules are more tightly coordinated by the electrolyte salt and therefore less prone to react with the electrode materials. Another approach is using solvents such as sulfones and nitriles, which are stable up to high potentials. These molecules, however, often possess a high viscosity which makes the ion conductivity low. One such example is sulfolane $(CH_2)_4SO_2$, see Fig. 3, which is a cyclic sulfone that has been used in electrolytes having an oxidation stability of >5.5 V vs. Li^+/Li.[29] The viscosity of sulfolane is 10.35 cP at 30 °C, which is high as compared to the other common solvents having 2.2 cP, 0.59 cP and 0.75 cP for PC, DMC and DEC, respectively.[30,31,32] It also has a melting point of 28 °C, thus being solid at room temperature.[33]

Battery safety is an important issue which is generally related to the properties of the electrolytes. Primarily, it is highly desired to avoid accidents where batteries catch fire – the battery contains stored energy and flammable materials, and can therefore burn. One way of achieving higher safety is using an SPE, where a solid polymer is used both to separate the electrodes and to transport ions, instead of a separator filled with highly flammable organic solvents. SPEs can also mitigate the problem with lithium dendrites if their mechanical strength is high enough – the electrolyte rigidity makes it difficult for the sharp dendrites to force their way through from the negative to the positive electrode. Ion conduction in solid state materials is, however, usually slow, which is also the case in LIBs utilizing SPEs. In order to increase the ionic conductivity, SPE batteries can be operated at a higher temperature, as the polymer chains then are more flexible. Practically, SPE cells are therefore often used where the temperature is around 60 °C or higher.

In commercial batteries, many different electrolyte additives are also included. These serve different functions, such as forming a stable solid electrolyte interphase (SEI), decreasing the flammability and preventing overcharging. Overcharging, for example, is prevented via oxidation of the additive on the positive electrode followed by diffusion to the negative electrode where

reduction takes place. The redox potential of such an additive must therefore be higher than the upper cut-off potential during cycling, otherwise the capacity of the cell will be reduced.

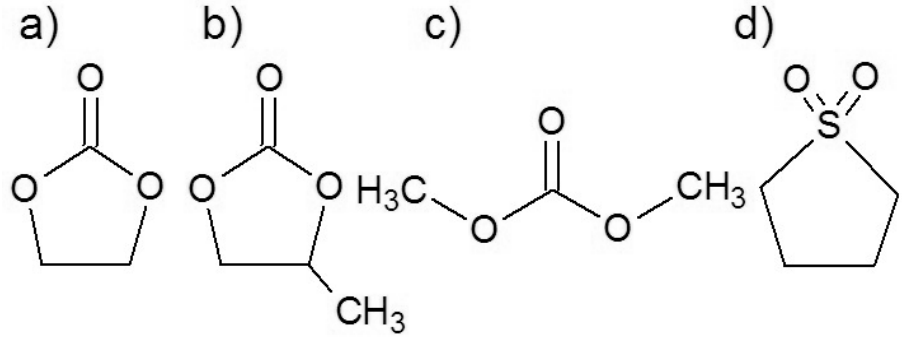

Figure 3. Different electrolyte molecules. a) Etylene carbonate. b) Propylene carbonate. c) Dimethyl carbonate. d) Sulfolane.

1.4 Separators

The purpose of the separator is to prevent direct physical contact between the positive and the negative electrodes, while allowing electrolyte to pass through. The separator is typically a thin porous film, consisting of e.g. polypropylene. Surface modifications can be used in order to increase the wettability. Wettability is important since if the pores in the separator will remain dry, it will prevent lithium ion transport and thereby increase the resistance.[34]

1.5 The Interphase between Electrode and Electrolyte

As stated above, in order to have a high energy density of a cell, a large potential difference between the positive and negative electrodes is required.[35] However, this requires that the electrochemical stability window of the electrolyte matches the large potential difference between the electrodes; see Fig. 4a.[28] The electrolyte's lowest unoccupied molecule orbital (LUMO) should be higher than the potential of the anode while its highest occupied molecular orbital (HOMO) should lie lower than the potential of the cathode in order to avoid spontaneous reactions. The potential of the cell will otherwise be limited by the potential at which the electrolyte participates in degradation reactions with the electrode, as illustrated in Fig. 4b. The case where a standard electrolyte, consisting of 1 M $LiPF_6$ salt in a solvent of carbonate-based hydrocarbons in a cell where lithium metal is cycled vs. NMC is illustrated in Fig. 4c. While the NMC remains in the electrochemical stability window, the lithium foil ex-

ceeds the limit. Despite this, such a cell can still cycle without complete degradation of the electrolyte, because a passivating Solid Electrolyte Interphase (SEI) layer will be formed on the lithium foil.[36] The SEI layer allows conduction of lithium ions but is electronically insulating, which prevents further reactions of the lithium foil with the electrolyte. However, cracks in the SEI and solvent molecules diffusing through it will cause a continuous degradation of the electrolyte. If the NMC electrode was cycled vs. LTO instead of lithium, both electrodes would remain in the electrochemical stability window of the electrolyte. There should, in theory, then be no degradation reactions, but at the cost of a smaller potential range within which the cell can be cycled. Even though the electrolyte is within the electrochemical stability window put up by the electrodes according to reference measurements, degradation reactions might still appear due to or catalytic effects of the electrode materials, which can affect the stability limit.[37]

Similarly, for the positive electrode, if it operates at a higher potential than the electrochemical stability window, the electrolyte will degrade. The degradation products should ideally remain at the electrode to allow lithium ion conduction, but being electronically insulating to prevent further degradation.

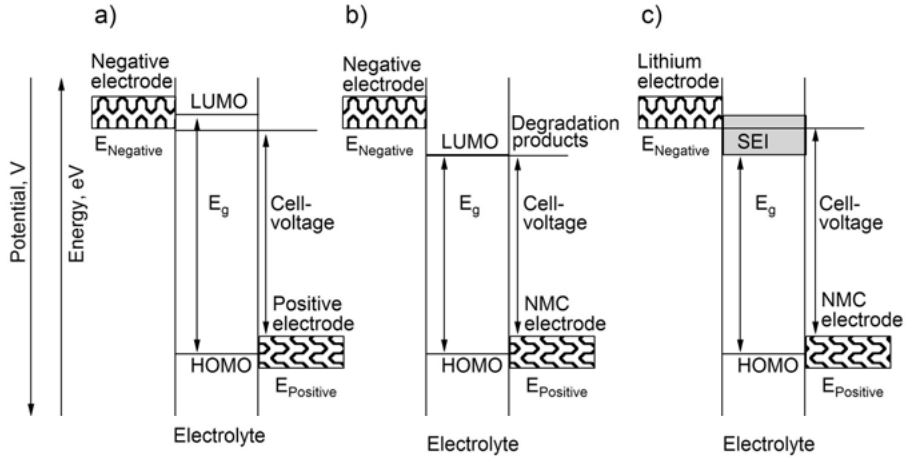

Figure 4. Electrochemical stability window of a typical LIB electrolyte in contact with electrodes. a) The stability window exceeds the potential differences between the electrodes. b) The negative electrode is outside the stability window, where no stable SEI is formed. c) The negative electrode is outside the stability window, but a stable SEI layer is formed.

1.6 Li-Ion Battery Ageing

As stated previously, battery ageing contribute substantially to cost and sustainability for the electrification of the transport sector. From a user perspective, LIB ageing will appear primarily as a decrease in capacity and voltage; i.e., that the battery needs to be recharged more often, and cannot provide enough power to do the required task and will not be able to deliver enough energy. When an LIB can only reach ca. 80% of its initial capacity, the ageing often starts to accelerate rapidly.

Battery ageing is related to a number of different independent and interdependent mechanisms in the LIB, schematically illustrated in Fig. 5. During cycling and storage, degradation will take place in the LIBs which decrease their performance. The type and amount of degradation depends on the cell chemistry, as well as operation conditions such as temperature, potential range, or C-rate.

1.6.1 Degradation Mechanisms at the Electrode-Electrolyte Interface

Manganese dissolution is a common ageing mechanism taking place in many positive electrode materials. The Mn will dissolve from many transition metal oxide electrodes, then migrate to the negative electrode where it deposits. The dissolution will decrease the capacity of the positive electrode and also affect the surface layer formation on the negative electrode. Mn will affect the impedance of the anode surface layer and also cause more side reactions with the electrolyte. It has been reported that Mn will either be reduced to metallic particles[38,39] or be present in its ionic state[40] on the negative electrode. Especially Mn(III) is problematic in this context: at the surface of the positive electrode it can undergo a disproportionation reaction into Mn(IV) and Mn(II), where after Mn(II) dissolves into the electrolyte.[41] Mn dissolution depends on several parameters; primarily high operation temperature, high potential used[42,] and presence of acids in the electrolyte.[43] It can be prevented by surface coatings or doping of the material which stabilizes the surface crystal structure.[44]

Lithium plating is another common degradation mechanism in LIBs. During lithium plating, metallic lithium will be deposited on the negative electrode instead of lithium ions being intercalating into it. Cycling a cell using high C-rates, cycling at low temperatures or cycling in a high SOC range severely increase the risk of lithium plating.[45] These cycling conditions might force the potential of the negative electrode below 0 V vs. Li^+/Li, making lithium plating thermodynamically favorable.[46] Lithium plating can be avoided by designing the cell so that the negative electrode has a larger capacity than the positive electrode,[47] or using a negative electrode having a somewhat higher operation potential. Long term effects of lithium plating are increased

amount of side reactions, increased impedance and decreased cell capacity, which all significantly age the battery .[46]

Formation of lithium dendrites affect both the safety of the LIB as well as cause side reactions which contribute to ageing.[48] The formation of dendrites is not only limited to lithium metal electrodes; they can also form on graphite. If graphite is over-lithiated, lithium nucleation and growth of dendrites will occur at its surface. The dendrites are very reactive towards the electrolyte and can form many degradation products. They can puncture the separator as they grow, leading to an internal short-circuit of the cell. Creating electrodes having a high electric conductivity can mitigate local over-lithiation and thereby prevent formation of dendrites.[49] Also addition of various film-forming additives have improved the performance due to a formation of a better SEI, although the detailed mechanisms are still not known in detail.[48]

Graphite exfoliation is detrimental for polycrystalline graphite electrodes having a high degree of graphitization, and cause ageing through rapid capacity decay.[50] The phenomenon depends on the electrolyte solvent, where for example PC is well known to co-intercalate into the graphite structure and cause exfoliation, whereas the cycling will proceed without exfoliation if EC instead is used.[51] Formation of a stable SEI layer can suppress exfoliation.[50]

Charging a positive material to high potentials might cause structural transformation of the surface of the active material.[42] Cycling to high potentials can therefore lead to a transformed surface layer, having higher impedance than the initial surface layer.[52] The transformed surface layer can be responsible for a poor coulombic efficiency during the first cycle, as well as causing capacity fading during cycling.[52]

Loss of active lithium is a common ageing mechanism causing capacity fading in LIBs.[53,54] In the case of loss of active lithium, the amount of useable lithium is consumed due to excess of reduction or oxidation side reactions, further explained in section 3.2.3.

1.6.2 Degradation Mechanisms in the Electrodes

Cation mixing is an ageing mechanism that primarily occurs at the LIB cathode. Usually, the mixing is caused by a transition metal ion which has changed position with a lithium ion. In the NMC material, cation mixing is considered to be thermodynamically favorable. Li^+ in the lithium layer then mix with the Ni^{2+} in the transition metal layer, depressing the Li^+ diffusion and cause the electrochemical performance to deteriorate.[55] Cation mixing is not necessarily bad for the battery; it can also stabilize the structure of transition metal oxides, increasing the rate capability and decreasing the lattice strain.[56] That the transition metal ions change their positions can also cause changes in the voltage slope, making it steeper. This is due to that in a material with large cation disorder, the Li^+ will experience different local transition metal environments.[57] Change of cation positions can also occur at the surface of particles

due to oxygen loss and transition metal migration; this has for example been seen on lithium nickel cobalt aluminum oxide (NCA).[58]

Loss of active material can occur on either or both of the electrodes and will lead to a decreased capacity, which cannot be utilized even if the battery is operated at lower rates. There are several possible degradation mechanisms causing loss of active material; e.g., it can be caused by dissolution of the active material,[59] structural transformation into an inactive phase[59] or by loss of contact where the active particle loses its electrical connection to the electrode. Loss of contact is often observed for electrode materials suffering from large volume changes during cycling, such as Si and Sn.[59] Loss of contact can also occur for positive electrode materials undergoing only limited volume changes during cycling, where instead degradation at high potentials and temperatures might form surface films which effectively insulates the particles.[59] The high potential might also degrade the electrode binder,[60] thereby causing loss of active material.

1.6.3 Degradation Mechanisms in the Electrolyte

There are many different ways electrolytes can degrade. Electrolytes containing $LiPF_6$ are sensitive to elevated temperatures, leading to formation of HF, which in turn can attack the electrodes and cause battery ageing. Interestingly, the HF formation at 60 °C has been found to depend on the solvent, where $LiPF_6$ dissolved in DEC will form more HF than if it dissolved in EC or PC.[61] Besides thermal decomposition the electrolyte can also be reduced or oxidized at the electrode, leading to formation of surface layers or dissolved reaction products.

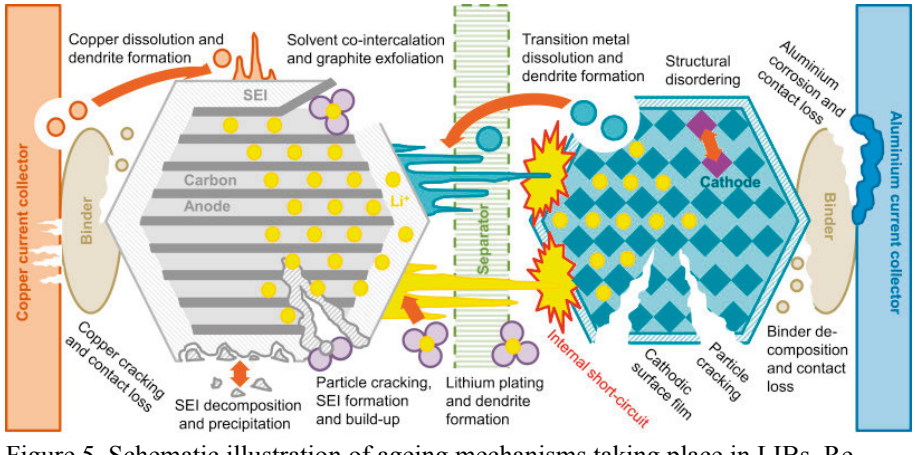

Figure 5. Schematic illustration of ageing mechanisms taking place in LIBs. Reprinted from Birkl et al., *Degradation diagnostics for lithium ion cells*, J. Power Sources **2017**, 341, 373-386, http://dx.doi.org/10.1016/j.jpowsour.2016.12.011, with permission from Elsevier.

2. Lithium Nickel Manganese Cobalt Oxide as a Cathode Material

The cathode material NMC is commonly used in commercial applications which require long life time, high energy density and high level of safety for the battery, such as in electric vehicles. NMC either has a higher practical specific capacity[62] or operates at a higher potential than competitor materials like LMO or LFP, making the energy density higher. The smaller amount of cobalt as compared to LCO makes NMC cheaper and more sustainable.[63,11] The atomic structure is layered, see Fig. 6, allowing fast solid state diffusion and thus making it possible to use micron-sized particles instead of nano-sized. There are, however, other commercial electrode materials with faster rate capabilities, such as LMO. Obtaining higher rate capabilities of NMC-containing electrodes is therefore possible by incorporation of LMO particles, i.e. blended electrodes of NMC and LMO[64], which are often used commercially. During charging of an NMC cell, the nickel ions are oxidized from +II to +IV, the cobalt ions are oxidized from +III to +IV whereas the manganese ions generally retain their initial oxidation state of +IV.[9]

The theoretical specific capacity of NMC (280 mAh/g) is not utilized in commercial applications. In order to reach close to this capacity, a high cut-off potential would be required. However, at the potential of 4.3 V structural degradation of the NMC start to take place[65] and a spinel-like phase is formed, especially on the surface. At higher cut-off potentials, e.g. 4.6 V, this effect is more pronounced, leading to a more rapid capacity fading.[65] Therefore, the upper cut-off value is often close to 4.3 V, at which about a capacity of ca. 160 mAh/g can be achieved.[65] Other structural degradations in NMC have also been observed, where the surface structure of the NMC have transformed into rock salt structure.[66] This thin layer has poor ionic and electronic conductivity, thus decreasing the capacity retention during battery cycling. It has also been shown that a thin film coating of the NMC particles can prevent structural degradation, allowing improved rate capability and cycle life.[64]

Transition metal ion dissolution can take place in NMC electrodes, where nickel, cobalt or manganese leave the NMC material by dissolving into the electrolyte. Ultimately, they can diffuse to the negative electrode where they cause imperfections in the SEI layer, thereby increasing the resistance in the battery.[67,68] The transition metal dissolution depends on cut-off potential, and a lower cut-off potential can decrease this problem.[67] Also the purity of the

electrolyte is important, as $LiPF_6$ can react with trace amounts of water forming HF, which is known to increase the rate of transition metal dissolution. One advantage of NMC over LMO electrodes is that the amount of transition metal dissolution in NMC is less than the manganese dissolution in LMO. It has also been shown that in blended electrodes of NMC and LMO, that NMC suppresses the manganese dissolution of LMO.[69]

As the NMC particles are cycled, stress will arise within them, causing micro-cracks to appear near defects or grain boundaries.[70] This phenomenon leads to continuous generation of surface where side reactions can take place, and cracked particles might also lose contact to the current collector causing capacity fading.[71]

Despite NMC having a larger capacity than many other positive electrode materials, it is beneficial to increase it further. This has been achieved via increasing the nickel content, while decreasing the amount of cobalt and manganese. Increasing the nickel content increases the main ion responsible for the redox reaction, thereby increasing the specific gravimetric capacity to about 200 mAh/g for $LiNi_{0.6}Mn_{0.2}Co_{0.2}O_2$ (also known as NMC (622), due to its transition metal composition). This will also decrease the amount of scarce cobalt used in the LIBs. Unfortunately, the increased nickel content will make the electrode surface more reactive towards the electrolyte.[71] There are several strategies to mitigate this problem, e.g. coating the particles with inactive material,[72] coating the particles with a different active material with higher stability,[73] or by synthesizing NMC having a nickel-rich core with a composition gradient so that the nickel content will be low at the surface.[74]

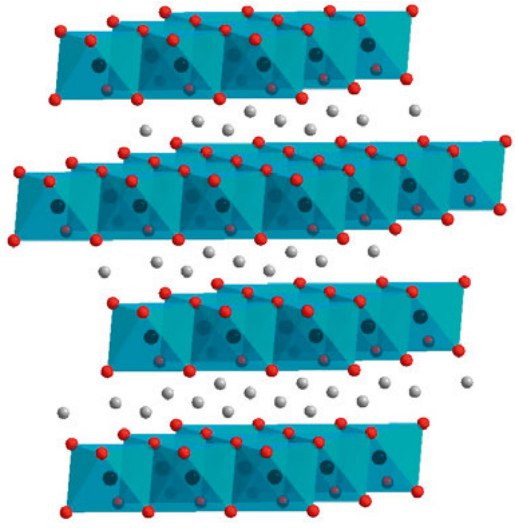

Figure 6. The crystal structure of NMC. Nickel, manganese and cobalt atoms are in black, lithium in grey and oxygen in red. The lithium atoms are positioned in layers in between oxygen atoms, the transition metals in the center of the polyhedra and the oxygen atoms at the corners of the polyhedra.

2.1 Scope of this Thesis

This thesis work aims at achieving a better understanding of cycle life in commercial cells for electric vehicles by finding out what factors limit the system and cause battery ageing. The work is mainly focused on the positive electrode, with NMC (111) and NMC (622) as the primary research area, since NMC electrodes are commonly utilized in commercial batteries. Less research has also been done of its ageing as compared to graphite anodes. Moreover, other materials such as LMO and graphite which are present in commercial cells are also studied to some extent.

It is well known that surface layer formation take place on both electrodes in an LIB, leading to increased resistance and capacity fading. This work therefore tries to increase the understanding of how these surface layers are affected depending on the electrode and electrolyte type in the cell and the cycling protocol performed. For these studies, x-ray photoelectron spectroscopy (XPS) has been one of the main characterization techniques for studying the surface layers of the electrodes, combined with other spectroscopic techniques such as hard x-ray photoelectron spectroscopy (HAXPES) and x-ray absorption near edge spectroscopy (XANES) in order to receive information about the chemical composition and oxidation state deeper into the electrode/electrolyte interphase.

The thesis comprises five different papers. In Paper I, it is investigated how the choice of negative electrode will affect the degradation products formed on the NMC electrode. In Paper II, the role of the temperature on the electrochemical performance and the electrolyte degradation is explored, finding out how the capacity fading is related to electrolyte reduction despite cycling within the ESW of the electrolyte. In Paper III and Paper IV, the use of EC-free electrolytes containing PC or sulfolane, respectively, are investigated for cycling at high potentials and low temperatures. In Paper V, it is studied how the position of a narrow SOC interval affects manganese dissolution, the chemistry of the surface layers as well as the individual electrochemical performance of the electrodes.

3. Methods

3.1 Electrode Preparation and Cell Assembly

The laboratory made NMC electrodes used in these studies were prepared in-house from slurry. The electrode slurry was a mixture of NMC, carbon black and binder at an 80:10:10 mass ratio. After ball milling, the slurry was casted on carbon coated aluminum foil using a pilot line, making it possible to control the thickness. The electrodes were punched out into discs that were individually pressed by applying a static pressure. To remove adsorbed water, the electrodes were dried in a vacuum oven in an argon filled glovebox.

Graphite electrodes were prepared from a slurry consisting of graphite, carbon black and super C65, binder (carboxymethyl cellulose (CMC), Styrene-Butadiene Rubber (SBR)) and water as solvent. The slurry was ball milled and coated on copper foil.

In cases where cells were constructed from commercial electrodes, the double-sided coating had to be removed first. Commercial cells were opened and disassembled in an argon filled glove box. The coating from one side was removed by a solvent infused tissue. NMP was used for the NMC/LMO electrodes whereas methanol was used for the graphite electrodes. Thereafter, discs were punched out for cell assembly.

The cells were assembled in a pouch cell format, where the electrodes were stacked between a Celgard separator soaked with electrolyte. Often, a LP40 electrolyte was used, consisting of 1 M $LiPF_6$ in EC and DEC in a 1:1 volume ratio.

3.2 Electrochemical Characterization

3.2.1 Galvanostatic Cycling

All cells investigated were allowed to rest for at least 12 hours in order for the electrolyte to infiltrate the electrodes. Thereafter, galvanostatic cycling was used to characterize the cells electrochemically. The cells were cycled using a Novonix High Precision Charger battery testing system, allowing precise measurements of current and temperature.

During galvanostatic cycling, a constant current is applied. The current remains constant until a certain cut-off potential is reached, at which the current

is reversed. It is also possible to define when the current should be reversed by the cell's state of charge (SOC). The potential interval where faradaic reactions take place in the electrodes is usually defined as the whole SOC range, i.e. 0-100% SOC. When the cell is fully charged the SOC is at 100%, whereas when it is fully discharged it is at 0% SOC. By applying this definition, it is possible to also cycle cells in limited SOC intervals by limiting the charge/discharge time until the current is reversed, instead of using fixed potential limits. The battery is cycled for a set number of cycles between these two cut-off potentials (or in a SOC range) at a certain speed (equivalent to current), usually referred to as C-rate. The C-rate corresponds to the time it takes to discharge the battery; e.g. if it takes 5 hours to discharge, the C-rate is C/5. Higher rates than 1C can also be expressed, where for example a C-rate of 4C corresponds to complete discharge of the cell in 15 minutes.

3.2.2 Incremental Capacity Analysis (ICA)

ICA is performed by plotting the differential capacity as a function of potential. In order to get detailed information from both the positive and the negative electrodes, the commercial cells were disassembled and reassembled into half-cells with lithium as counter/reference electrode. Lithium is considered to have a constant potential independent of the current, which is used as assumption so that the analyzed signal only depends on the working electrode. The data obtained from galvanostatic cell cycling can be converted into ICA plots. However, the C-rate should be low, otherwise the potential of the counter/reference electrode might change. Additionally, the response from the working electrode will not only depend on the electrode material, but also on kinetic effects of the system. In Fig. 7 it is seen how the peaks observed in ICA plots correspond to constant potential plateaus in the potential vs. capacity plots obtained from galvanostatic cycling. This method can identify and quantify ageing phenomena such as increased over-potential and loss of active material. In the case of loss of active material, the intensity of all peaks coming from that material would decrease proportionally to their initial value, whereas in the case of increased over-potential the distance between the lithiation and delithiation peaks would increase. In a blended electrode, such as NMC/LMO studied here, the technique can therefore be used to distinguish which of the material that degrades the most. Changes in cell resistance can be obtained from observation of changes in the potential at which the peaks appear.

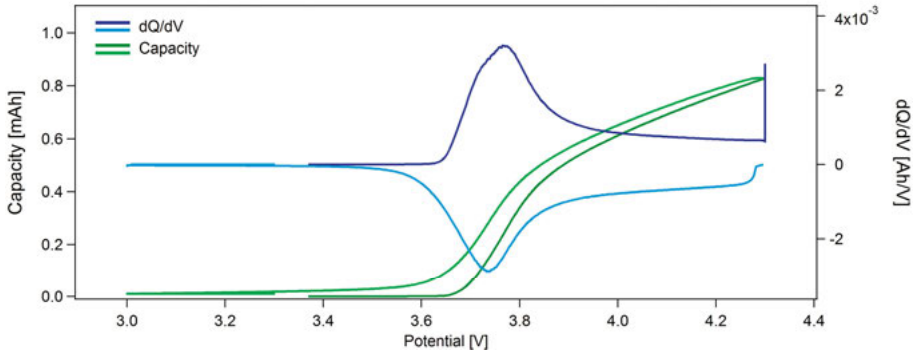

Figure 7. Incremental capacity plot of NMC vs. Li, where dark blue and light blue depicts the delithiation and lithiation of the NMC, respectively. The green curves show the corresponding capacity plot where dark green and light green depicts the delithiation and lithiation of NMC, respectively.

3.2.3 Electrode Slippage

To balance cells, the capacity of the individual electrode materials are often used. This does, however, not necessarily correspond to the utilized capacity of the full-cell. In a full-cell, the capacity can be limited despite that one of the electrode materials is not fully lithiated/delithiated. The limited capacity is instead caused by side-reactions that lead to that the potential window of the electrodes 'slip' relative to each other. By measuring the slippage, the amount of side-reactions can be estimated.

In the case of electrolyte reduction of solvent at the negative electrode, an electron is consumed from the electrode. To maintain charge neutrality, the electrode must either receive a negative charge or give away a positive charge. This can be done by a lithium ion moving out of the electrode or an electron moving from the other electrode. This electrode in turn becomes charged, and has to compensate this by a lithium ion moving out of the electrode; see Fig. 8. Oppositely, in the case of electrolyte oxidation an electron will be received by the electrode, leading to that either a positive charge have to enter the electrode or it has to give away a negative charge to remain the charge neutrality. A lithium will therefore move into the positive electrode or the electrode will give away an electron to the negative electrode followed by lithium insertion into the negative electrode.

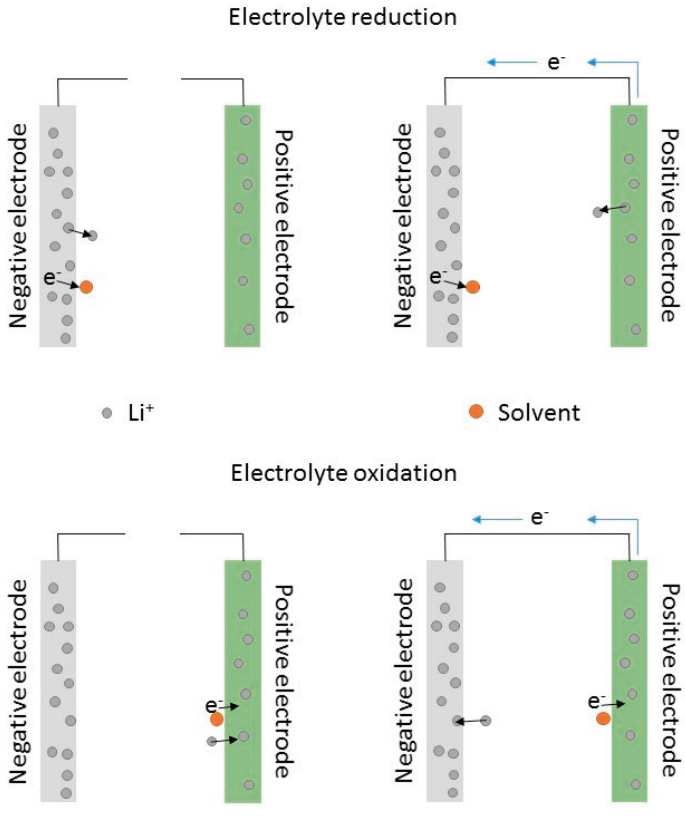

Figure 8. Schematic representation of electrolyte reduction and oxidation, illustrating how lithium ions will be received or released.

During either oxidation or reduction of the electrolyte, the side reactions will cause a change of lithium concentration in only one of the electrodes. Hence, only one of the electrodes will change its potential. During electrolyte reduction the negative electrode will either loose one lithium ion, i.e. the negative electrode's potential increases, leading to a slippage of the electrode to the left, see Fig. 9, or the positive electrode will lose one lithium ion, thereby increasing the potential and leading to a slippage of the positive electrode towards the right. Both these scenarios will lead to the same slippage of the electrodes relatively to each other. The slippage will then limit the discharge capacity as the negative electrode will be fully delithiated, while the positive electrode has unused capacity left.

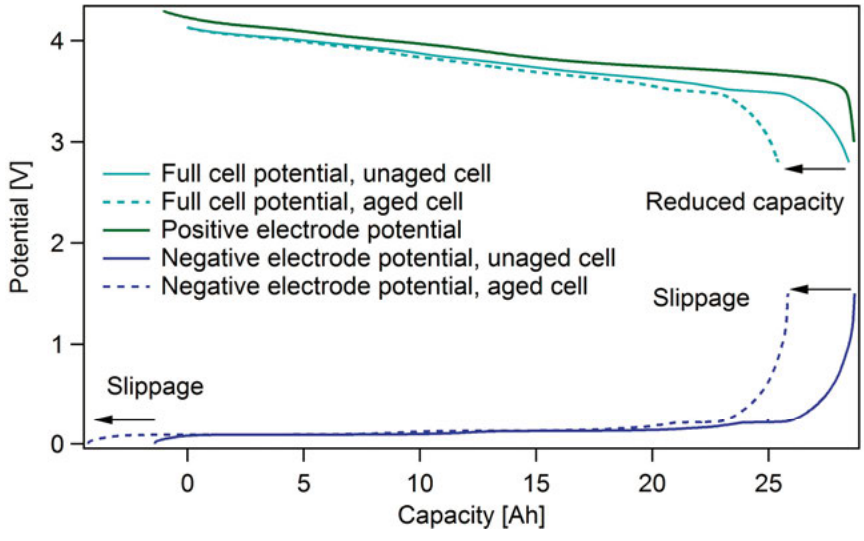

Figure 9. Schematic representation of how the electrodes will slip during electrolyte reduction, leading to a reduced capacity.

3.3 X-Ray Photoelectron Spectroscopy (XPS)

XPS is a commonly used electron spectroscopy method for analysis of surfaces. It is also referred to as electron spectroscopy for chemical analysis (ESCA)[75] and was extensively explored by Kai Siegbahn, for which he received the Nobel Prize in 1981.[76] XPS can differentiate between elements as well as elements in different compounds. The working principle of XPS is based on the photoelectric effect.[77] As a photon meets a sample, different phenomena might occur. In one of these, the incoming photon transfers its energy to the atom and knocks away a core level electron. The kinetic energy of the emitted electron will depend both on how tightly it was bound and the energy of the incoming photon, described in Fig. 10.

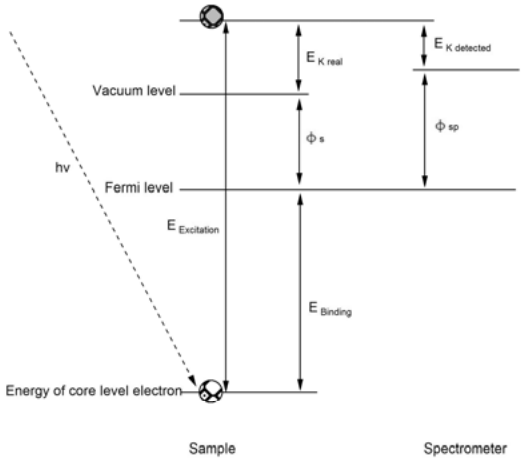

Figure 10. Schematic illustration of the detection of the binding energy, where $E_{K\ real}$ is the real kinetic energy of the electron, $E_{K\ detected}$ is the detected kinetic energy of the electron, ϕ_s is the work function of the sample, ϕ_{sp} is the work function of the spectrometer and $E_{Binding}$ is the binding energy of the electron.

The binding energy can therefore be calculated according to Equation 1:[78]

$$h\nu = E_K + E_B + \phi_{sp} \qquad (1)$$

where hν is the energy of the incoming photon, E_K is the detected kinetic energy of the emitted electron, E_B is the binding energy of the electron and ϕ_{sp} is the work function of the spectrometer. The incoming energy of the photon is generally known in an experiment; usually (as in several of these studies) it is $Al_{K\alpha}$ at the energy of 1486.6 eV.[79] Since the kinetic energy of the electrons is determined in the analyzer, and the work function of the spectrometer is known, it is possible to calculate the binding energy. The binding energy is dependent on the electron orbital of the element but also shifts depending on what atoms this element is bound to. The shift taking place due to how the element is bound is useful for identifying different chemical compounds. In a molecule, a shift towards higher binding energy would appear if it contains strongly electronegative atoms. The electronegative atoms would then draw electrons from the other atoms, thus making the remaining electrons in the atom more tightly bound.

To detect the photoelectrons, a concentric hemispherical analyzer is used, allowing only electrons of certain energy to pass through. This pass energy depends on the potentials applied to the different hemispheres, whereas the resolution depends on the pass energy[80] and the radius of the hemispheres. In order to avoid large detectors and different resolution depending on electron

energy, the pass energy is set to a constant value and electrons are retarded before reaching the analyzer; i.e. the retardation of the electrons are measured. In a spectrum of a homogeneous sample, the intensity of the photoelectrons per second can be described by Equation 2:[81]

$$I = nf\sigma\phi\gamma AT\lambda \quad (2)$$

where n is the number of atoms per volume unit, f is the flux of incoming photons, σ is the photoelectric cross section, ϕ is based on the angle between the incoming photons and emitted photoelectrons, γ is the efficiency in the photoelectric process for production of photoelectrons of the normal photoelectron energy, A is the area of the sample emitting photoelectrons which are detected, T is the detection efficiency and λ is the mean free path of the photoelectrons in the sample. The equation can be simplified by introducing a sensitivity factor S, described by Equation 3:[82]

$$S = f\sigma\phi\gamma AT\lambda \quad (3)$$

The sensitivity factor is often experimentally determined and is listed in handbooks. It can be used for quantification of the elements according to Equation 4:[83]

$$C_{element} = \frac{n_{element}}{\Sigma n_{All\ elements}} = \frac{\frac{I_{element}}{S_{element}}}{\Sigma\frac{I_{element}}{S_{element}}} \quad (4)$$

where $C_{element}$ is the atomic percentage of a certain element, $n_{element}$ is the number of atoms of a certain element in the analyzed volume and $S_{element}$ is the sensitivity factor.

3.4 Hard X-Ray Photoelectron Spectroscopy (HAXPES)

The working principle of HAXPES is similar to XPS. However, HAXPES gives information about composition from a larger depth of the surface.[84] It is possible to receive photoelectrons from deeper into the sample because HAXPES utilizes 'hard' X-rays, having energies of 2 keV or higher.[85] The energy of the incoming photons determines the kinetic energy measured according to Eq. 1. Higher photon energy would therefore increase the kinetic energy of the photoelectrons, thereby increasing the inelastic mean free path of the electrons. The dependency of the inelastic mean free path of electrons as a function of kinetic energy can be seen in Fig. 11. The shape of this curve differs slightly depending on the material containing the photoelectrons, but the trend nevertheless remains.

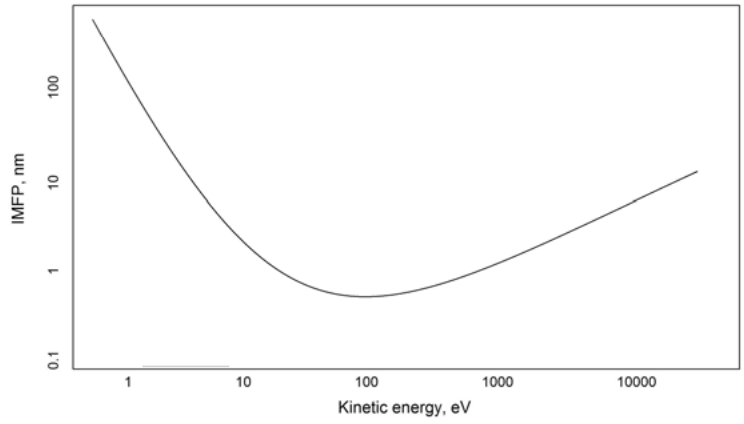

Figure 11. Schematic representation of the inelastic mean free path as a function of kinetic energy.

The high energy of the X-rays necessary for HAXPES usually requires the measurements to be performed at a synchrotron facility. In some of the studies in this thesis, measurements were performed at the KMC-1 beamline at BESSY where it is possible to tune the energy between 1.7 keV to 12 keV.

3.5 X-ray Absorption Near Edge Structure (XANES)

XANES is a useful technique to compare oxidation states of ions in different samples.[86] Additionally, information about the three-dimensional structure around the ion can be obtained.[87] Instead of using a constant energy of the incoming photons as in XPS, the energy of the photons is changed in XANES.[88] The photon energy is swept from a value lower than the energy required in order to knock out photoelectrons of a certain binding energy from a core level, and increases past the required energy.[89] The obtained signal is therefore initially close to zero as no photoelectrons are emitted, but increases as the energy at which photoelectrons are excited increases. The energy range at which the photon absorption changes from almost zero to a high value is referred to as 'the edge'. The photoelectron will in this range interact with neighboring atoms before it is absorbed, which thereby gives qualitative information on the surroundings.[87] In the setup used in this study, the recorded signal comes from X-ray fluorescence taking place as an excited ion relaxes. The position of the edge corresponds to how tightly the electrons are bound to the atom, and hence is largely influenced by the oxidation state; see Fig. 12.[90] The higher the oxidation state, the more the position of the edge will shift towards higher energies.[91]

The XANES region of an absorption spectrum is sensitive to small variations in structure. The electrons which are excited close to the edge have a low kinetic energy[92,93,94] and therefore also a long inelastic mean free path. This will lead to interactions further away from distant atoms than observed in extended x-ray absorption fine structure (EXAFS) spectra.[87] The sensitivity to structural differences is partly caused by geometrical differences between the different scattering sites. A different geometry would lead to different scattering pathways of the electrons, and therefore affecting the spectrum in the immediate area of the absorption edge.[95] Sometimes a 'pre-edge' before the edge in the spectrum can be observed. The pre-edge corresponds to specific orbital transitions, whose intensities might give information about the coordination number around the atom.[96]

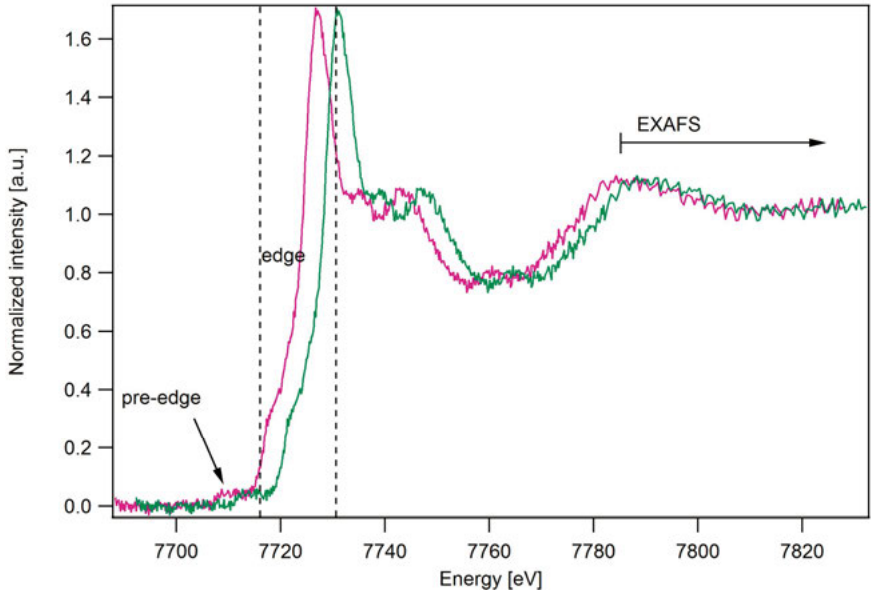

Figure 12. Schematic X-ray absorption measurements showing the different regions of the spectrum as well as differences in oxidation state between different samples, where the green spectrum corresponds to an ion in a higher oxidation state than the ion represented by the purple spectrum.

4. Results and Discussion

4.1 The Influence of the Negative Electrode on NMC-Based Cells

This section describes the role of the negative electrode on the performance of NMC-based cells. The aim was to analyze how the surface chemistry of the NMC electrodes was affected by various negative electrodes including lithium foil, graphite and LTO. The results presented in this section are based on Paper I.

4.1.1 Electrochemical Performance of NMC Electrodes Depending on the Negative Electrode

NMC cells with three different negative electrodes – lithium foil, graphite and LTO, respectively – were investigated by galvanostatic cycling in order to determine how the negative electrode affects their cycle life.

In the galvanostatic cycling results shown in Fig. 13, a large capacity fade is observed in the NMC-lithium cell, but only minor capacity fade is observed in the NMC-LTO and NMC-graphite cells. The rapid capacity fading observed in the NMC-lithium cell is unlikely due to loss of lithium in different side reactions, as the amount of lithium is in a large excess compared to the NMC electrode. It is shown in Fig. 13(d), which display the voltage hysteresis in the galvanostatic cycling curves, that the NMC-LTO and NMC-graphite cells have a stable and low voltage hysteresis while the NMC-lithium cell has an increasing hysteresis as the number of cycles increases. The increased voltage hysteresis is therefore likely the main cause for the capacity fading, as the cut-off potential would be reached before the cell is fully charged or discharged.

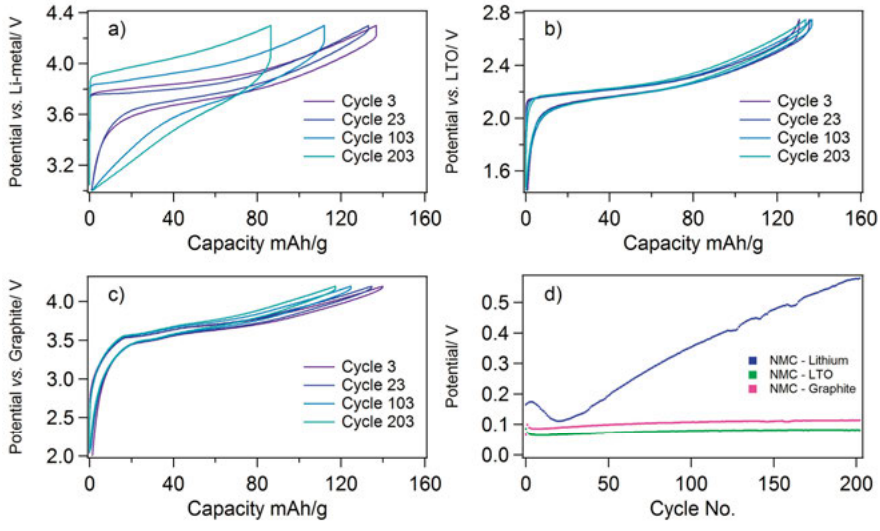

Figure 13. Galvanostatic cycles of NMC positive electrodes cycled towards different negative electrodes at 1C rate. a) Li-foil vs. NMC. b) LTO vs. NMC. c) Graphite vs. NMC. d) Voltage hysteresis vs. number of cycles.

4.1.2 XPS Results

In order to find out if any surface layer was formed on the NMC electrodes, XPS measurements were performed; see Fig. 14. In the O 1s spectra, the NMC-graphite and NMC-LTO cells show only minor differences, whereas the intensity is far larger in the range 533-534 eV for the NMC-lithium cell. This corresponds to electrolyte degradation products. The phenomenon can also be observed in the C 1s spectra, where a more pronounced peak is observed at 287-288 eV, corresponding to C-O, O-C-O or C=O species. In the F 1s spectra at 685 eV, on the other hand, a smaller amount of LiF is present in the NMC-lithium cell than in the NMC-LTO cell. Similarly, in the P 2p spectra a smaller amount of phosphorus degradation products is found in the NMC-lithium cells than the in NMC-LTO cells. The increased amount of phosphorus and fluorine degradation products seen in the NMC-LTO cells is likely to be caused by degradation of the $LiPF_6$ salt, which is the only source of phosphorus in the cell. If a uniform distribution of species is assumed, the results indicate a more organic surface layer in the NMC-lithium cells and a more inorganic surface layer in the NMC-LTO cells.

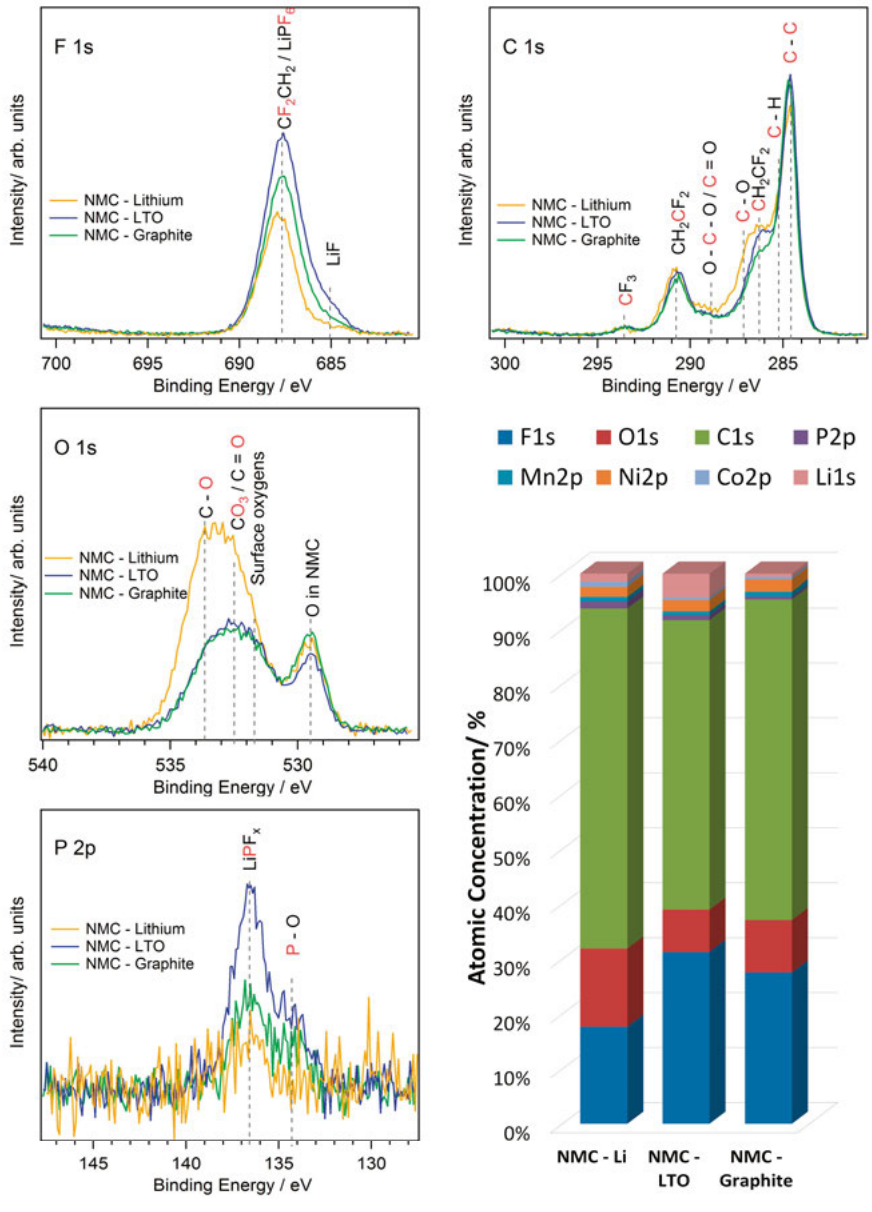

Figure 14. XPS spectra of NMC positive electrodes after 203 cycles in cells with different negative electrodes of graphite, LTO or lithium, and the relative atomic concentrations of different elements in the surface layer covering the NMC electrodes.

The surface layer formation process was also analyzed after different numbers of cycles to find out how the surface layer changes during battery operation. In Fig. 15, XPS measurements of a pristine NMC electrode are compared to electrodes cycled vs. lithium for 3 and 203 cycles. It is seen that there are only minor differences between the pristine electrode and the electrode cycled for 3 cycles, indicating that the surface layer is very thin after 3 cycles. In the O 1s spectra after 203 cycles, however, the intensity from two major peaks at 532.0 and 533.3 eV have appeared, representing carbonates such as Li_2CO_3 or $ROCO_2Li$ and polyethers. It is thus shown that the surface layer formation on the NMC electrodes takes place by repeated cycling for many cycles, further supporting that electrolyte degradation products are mainly formed on the negative lithium electrode and diffuse over to the positive electrode. This is likely the major cause of the poor capacity retention and increased voltage hysteresis observed in the NMC-lithium cell.

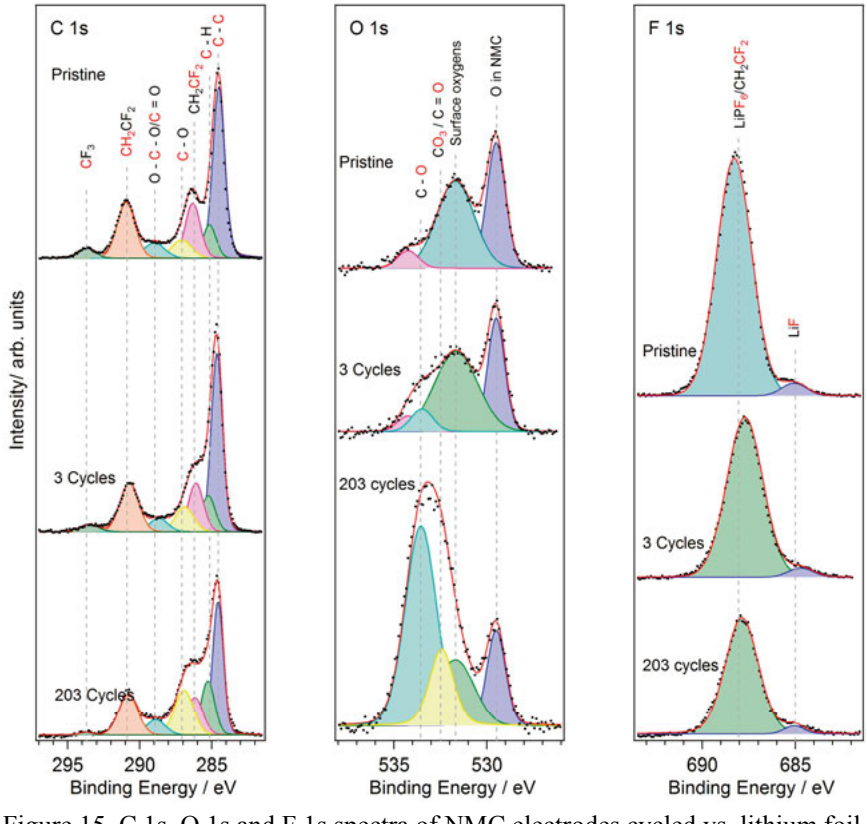

Figure 15. C 1s, O 1s and F 1s spectra of NMC electrodes cycled vs. lithium foil after different number of cycles.

4.1.3 Oxidation State Characterization of the 3d-Elements in NMC Electrodes

The oxidation state of the transition metal ions after long term cycling of the NMC electrodes was analyzed by XANES measurements. Fig. 16 shows the manganese, cobalt and nickel K-edges after different numbers of cycles. There are only minor differences in the manganese K-edge after cycling for 203 cycles compared to the pristine electrode. This indicates little change of oxidation state after cycling, which in other studies[97] has been determined to be +IV for similar structures. The electrode cycled for 203.5 cycles show differences in edge shape, indicating a change in the atomic environment around Mn during delithiation. Similarly for the cobalt K-edge, no major differences were observed between the pristine and the cycled lithiated electrodes, also indicating that the oxidation state remains unchanged. In the delithiated state the shape of the edge changes, indicating a difference in the environment around the cobalt ions. The nickel K-edge is similar for all lithiated electrodes, but differs in the delithiated state. The edge position of the delithiated electrode shifted towards higher energies, indicating an increase of oxidation state. These XANES results suggests that the oxidation state and environment around the transition metal ions remain unchanged in the lithiated state, even after cycling. The capacity fading in the NMC cells is therefore unlikely to be caused by structural deterioration of the transition metals in the bulk of the NMC particles, thereby supporting that surface layer formation on the electrodes is the cause of the low capacity retention.

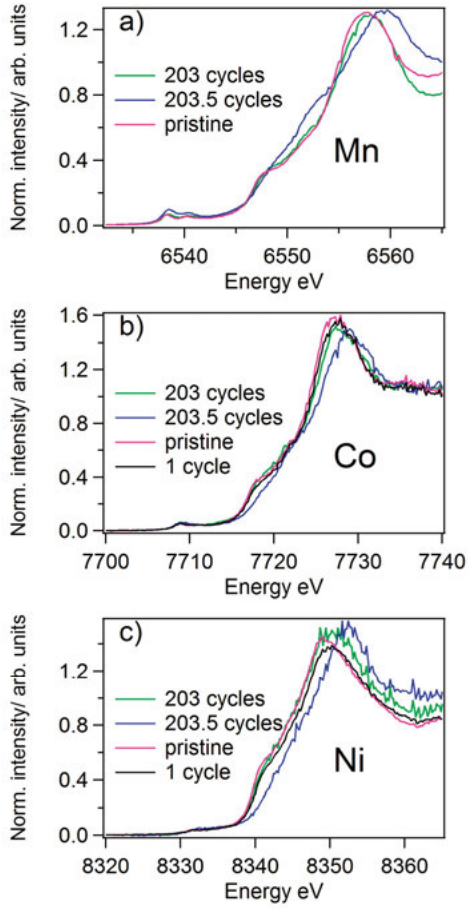

Figure 16. XANES measurements of the K-edge of different transition metals in NMC electrodes cycled vs. lithium. a) Manganese. b) Cobalt. c) Nickel.

4.2 How Temperature Affects Ageing

This section describes how the temperature affects ageing in NMC-LTO cells. The purpose was to characterize how electrolyte oxidation and reduction will affect the capacity retention during cycling, when using conventional cut-off potentials within the ESW of the electrolyte. The results in this section are mainly based on Paper III.

4.2.1 Cycling Performance

The cells were cycled at three different temperatures: 55 °C, 30 °C and -10 °C. In Fig. 17 it is seen that the capacity fading is minor when cycling at 30 °C, and significant at both 55 °C and -10 °C, although the initial capacity for

the latter was much lower. This correlates well with the coulombic efficiency, which is close to 100 % at 30 °C. This is despite the lower coulombic efficiency on the first cycles, indicating surface stabilization in the initial cycling. At 55 °C, the low coulombic efficiency of about 98 % indicates continuous side-reactions and the even lower coulombic efficiency at -10 °C is likely caused by side-reactions or possibly the large overpotential observed.

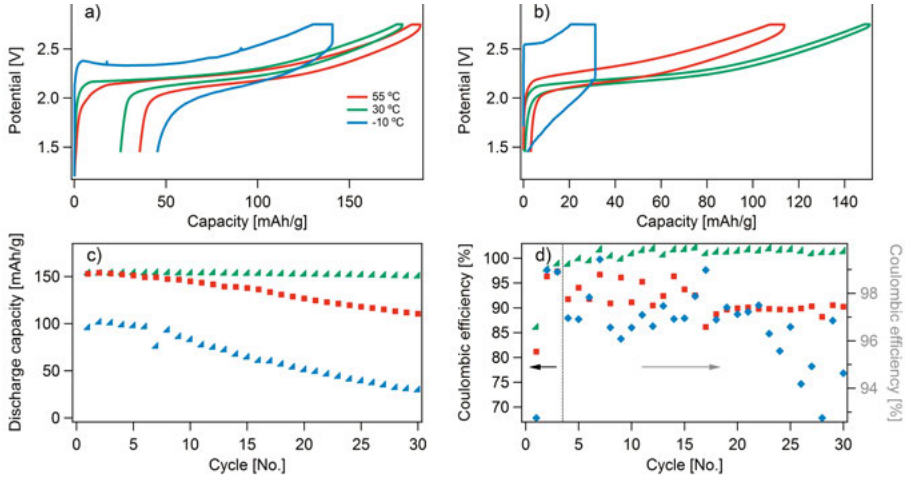

Figure 17. Electrochemical cycling of NMC-LTO cells operated at different temperatures. a) Potential profiles during the first cycle. b) Potential profiles during cycle no. 30. c) Discharge capacity vs. cycle number. d) coulombic efficiency vs. cycle number.

To find out what kind of side reactions take place at the individual electrodes, symmetric NMC-NMC and LTO-LTO cells were cycled, se Fig. 18. At -10 °C, the performance of all cells was poor, indicating that it is the low ionic conductivity of the electrolyte that limits capacity. At 30 °C, the LTO-LTO cell performed well with minor capacity fading, whereas the NMC-NMC cell showed clear fading which indicates that side reactions occur. The capacity fading of the NMC-NMC cell is interesting since the LTO-LTO cells and the NMC-LTO cells cycle without losing much capacity. This can possibly be explained by initial reduction of electrolyte impurities taking place at the LTO electrode, preventing these species from reacting at the NMC electrode. A possible alternative explanation is that reduced electrolyte species at the LTO electrode might diffuse over to the NMC electrode, forming a more stable surface layer. At 55 °C, capacity fading is observed for both LTO-LTO and NMC-NMC cells, even though it is worse for NMC-NMC. This indicates that the mechanism through which LTO is stabilizing the cycling of the full cell at 30 °C is not enough to suppress the side reactions at 55 °C.

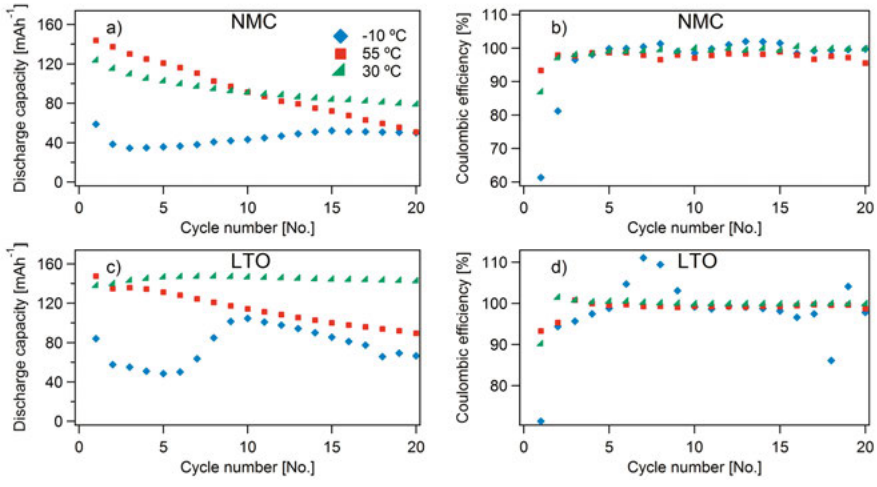

Figure 18. Cycling of symmetric NMC-NMC and LTO-LTO cells at different temperatures. a) NMC-NMC cells, discharge capacity vs. cycle number. b) NMC-NMC cells, coulombic efficiency vs. cycle number. c) LTO-LTO, discharge capacity vs. cycle number. d) LTO-LTO coulombic efficiency vs. cycle number.

To confirm whether it is oxidation or reduction side reactions that dominate, the LTO electrodes from the cycled cells were reassembled into new half cells. The open circuit voltage (OCV) was far higher than 1.55 V (which is the potential where LTO is delithiated) for the cells cycled at 30 °C and 55 °C, indicating that these electrodes are fully delithiated when the full cell is discharged. In other words, the LTO electrode will limit the discharge capacity of the cell. At -10 °C, the potential was close to 1.55 V, showing that the LTO electrode was not fully delithiated, likely due to the large over-potential as seen from the large voltage hysteresis in Fig. 17b.

The cell parameters of the NMC electrodes from the discharged full cells cycled 30 cycles were measured by X-ray diffraction (XRD). The cell parameters are useful for determining the degree of lithiation of NMC electrodes, as the unit cell expands along the c edge and contracts along the a edge during delithiation.[67,98,99] The amount of lithium in the electrodes was obtained by comparing the measured ratio between the c edge and the a edge.[100] The amount of lost lithium corresponds to X in $Li_{1-x}Ni_{0.33}Mn_{0.33}Co_{0.33}O_2$; see Table 1. In the cycled electrodes, 7.8 % is lost after cycling at 30 °C, 21.7 % is lost after cycling at 55 °C and 35% is lost after cycling at -10 °C. This confirms the OCV measurements of the LTO electrodes, i.e. that the LTO electrodes cycled at 30 °C and 55 °C are fully delithiated while the NMC could be lithiated further. The fully delithiated LTO and the incomplete lithiation of the NMC electrodes show that the electrodes have slipped relatively to each other, and that it is the reduction side reactions that is predominant since it is the

LTO electrode that limits the discharge capacity. At -10 °C neither of the electrodes are fully lithiated or delithiated, further supporting that it is the overpotential that limits the capacity.

Table 1. The ratio between the c edge and the a edge of the NMC unit cell, the amount of lost lithium and the weighted profile R-factor of the Le Bail fit.

Sample	c/a, Å/Å	Lost lithium, %	R_{wp}
Pristine powder	4.976	1.3	4.26
55 °C Cycling	5.052	21.7	6.24
30 °C Cycling	5.000	7.8	8.32
-10 °C Cycling	5.10	35	6.58

To characterize the side reactions taking place at the electrodes photoelectron spectroscopy (PES) measurements were performed. On the NMC electrodes, soft x-ray photoelectron spectroscopy (SOXPES) measurements were investigating the outermost surface (3 nm). Additionally, HAXPES measurements were performed to probe deeper into the material: 20 and 50 nm. In Fig. 19, the bulk peaks from the carbon black in the C 1s spectra at 285 eV and the metal-oxygen feature at 530 eV is present in all samples even during the SOXPES measurements, indicating that the surface layer on the electrodes is thinner than 3 nm.

The C 1s spectra show that there are various organic species formed on top of the electrode. The contribution from organic species is slightly higher at higher temperatures. LiF is seen in the F 1s spectra, and the HAXPES measurements indicate that these are deeper into the surface layer. The contribution from LiF decreases at higher temperatures, possibly due to the higher temperatures leading to increased solubility. At -10 °C the contribution from the metal-oxygen feature at 530 eV is larger in the O 1s SOXPES spectra than at the other temperatures, indicating formation of less organic species or formation of a thinner surface layer.

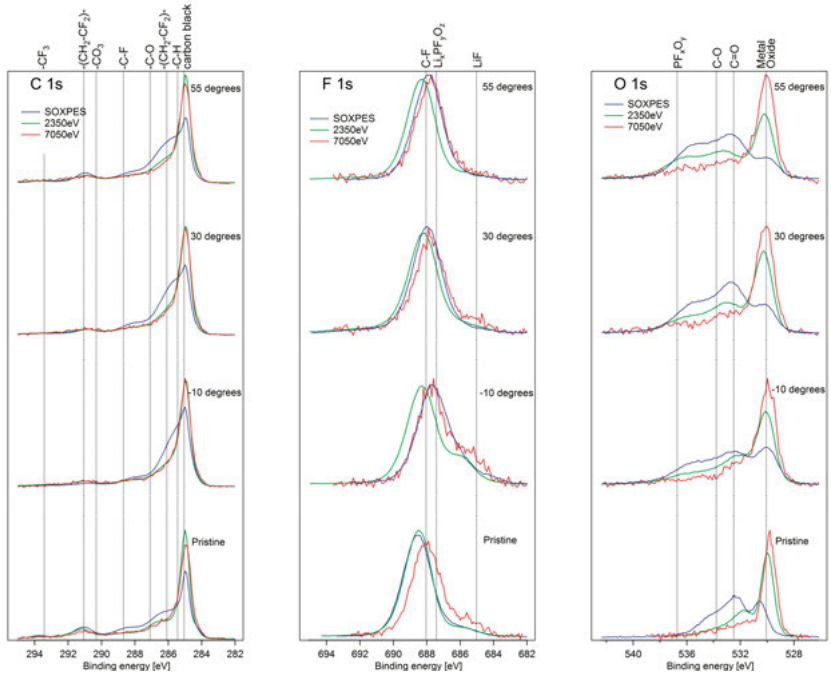

Figure 19. C 1s, F 1s and O 1s spectra of the NMC electrodes cycled 30 cycles.

From the relative atomic concentrations in Fig. 20, it is seen that the concentrations are very similar at 30 °C and 55 °C, but differs at -10 °C. At -10 °C, the relative amounts of fluorine and lithium is higher, whereas the relative amounts of carbon, oxygen and phosphorus are lower. In other words, more LiF and less organic species are formed at -10 °C.

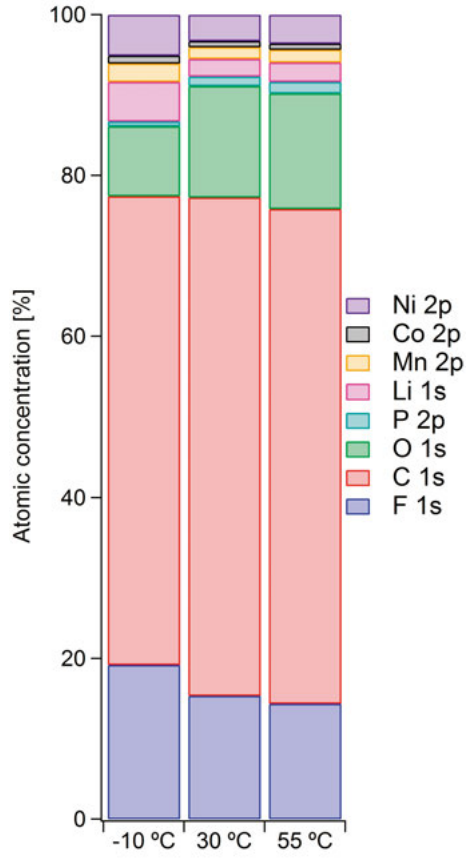

Figure 20. The relative atomic concentrations of the surface layers on NMC electrodes when cycled at different temperatures.

Fig. 21 shows the Ni $L_{II,III}$-edge and the Mn $L_{II,III}$-edge XANES spectra of the NMC electrodes. Two features are observed in all of the Ni L_{III} spectra at 854.7 eV and 856.4 eV, whose relative contributions correspond to the oxidation state:[101] a high intensity of the low energy peak indicates 2+, and a high intensity of the high energy peak indicates 3+. In the pristine and at the electrode cycled at 30 °C, much of the nickel seems to be present as Ni^{2+}, while more Ni^{3+} is present for electrodes cycled at -10 and 55 °C. This agrees well with the XRD measurements, which showed that cycling at -10 and 55 °C will not lithiate the NMC electrodes as much during discharge. Similarly, the Mn L_{III}-edge edge also consists of two main peaks, although both peaks correspond to Mn^{4+}. On the low energy side of these peaks, small features corresponding to Mn^{2+} and Mn^{3+} can be observed.[102,52] This might be caused by lattice reconstruction of the NMC into the rock salt structure.[52]

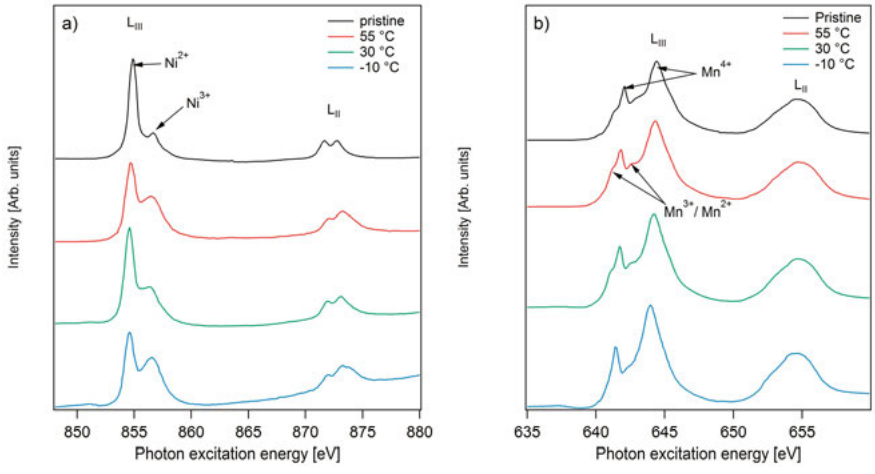

Figure 21. XANES spectra of the NMC electrodes after 30 cycles: a) Ni L-edge, b) Mn L-edge.

The LTO electrodes were analyzed with XPS to find out what kind of degradation products that would form. The reactions at the LTO electrodes should be the most interesting, since the OCV of the cycled LTO electrodes and the XRD measurements showed that it was mainly reduction processes taking place that would limit the capacity. Fig. 22 shows the O 1s, C 1s F 1s and P 2p spectra of the cycled LTO electrodes.

Similarly to the NMC electrodes, the carbon black and the metal-oxygen feature at 530.4 eV can be seen on all electrodes, indicating a surface layer thickness thinner than 9 nm. The C 1s spectra show peaks around 285 eV and 287 eV, corresponding to –C-H and –C-O, respectively.[103] At 55 °C the –C-H peak has a larger contribution than for the other temperatures, indicating formation of more hydrocarbons at elevated temperatures. The F 1s peak has contributions from three different peaks at 685.0 eV, 686.2 eV and 688.1 eV corresponding to LiF, Li_xPF_y/$Li_xPF_yO_z$ and $LiPF_6$, respectively. At -10 °C, the presence of Li_xPF_y/$Li_xPF_yO_z$ is much larger than at higher temperatures, possibly contributing to the large voltage hysteresis during the cycling. The P 2p spectra show a large peak at 135.5 eV, which mainly corresponds to the salt anion.[40] At -10 °C the contribution around 138 eV is slightly larger, likely coming from a different degradation product of the salt.

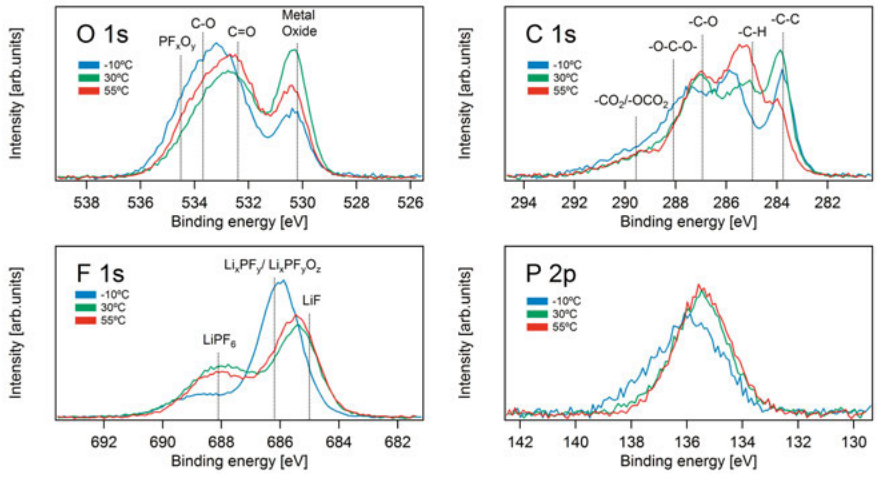

Figure 22. O 1s, C 1s, F 1s and P 2p XPS spectra of the LTO electrodes cycled 30 cycles.

From the relative atomic concentrations in Fig. 23 it is seen that the fraction of titanium varies between samples. It should only be present in the LTO particles as it is not expected to dissolve, and the titanium concentration is therefore an indication of the surface layer thickness. The low concentration at -10 °C suggest the thickest surface layer, whereas the high concentration at 30 °C indicates the thinnest surface layer. The larger relative atomic concentration of carbon at 55 °C further supports the increased amount of hydrocarbons formed. At -10 °C, the fluorine concentration is larger than for the other temperatures, also indicating that the formation of $Li_xPF_y/Li_xPF_yO_z$ is more pronounced.

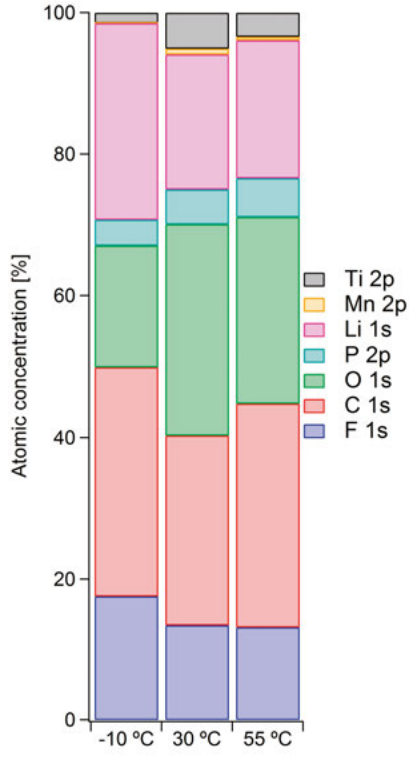

Figure 23. The relative atomic concentrations at the surface layers of LTO electrodes cycled at different temperatures.

4.3 How Electrolyte Solvent Affects Ageing

This section describes how the choice of electrolyte solvent affects ageing in NMC (622)-LTO cells. The purpose has been to study electrolytes without EC, as EC will be oxidized at high potentials but is less necessary as electrolyte component in cells not using graphite. The results are based on Papers III and IV.

4.3.1 Electrolyte Selection

It has previously been shown that linear low-M_w organic carbonates have good stability at high potentials.[104] Many linear carbonates also have a low viscosity, which is beneficial for a high conductivity, but have a too low dielectric constant which cause ion pairing. Linear carbonates can therefore be blended with a solvent molecule having a high dielectric constant. To this end, the high dielectric constant PC was chosen in combination with the low-viscosity DMC. From the conductivity measurements (Fig. 24) it is seen that the PC-

DMC mixtures achieve higher conductivity than the pure solvents and the EC containing reference electrolyte.

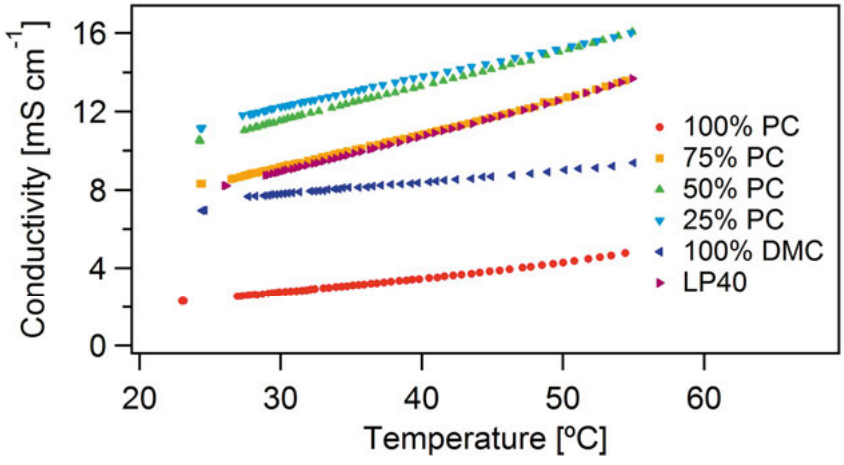

Figure 24. Ionic conductivity measured at different temperatures for electrolytes containing 1 M $LiPF_6$ in different ratios of PC and DMC as well as LP40 (1M $LiPF_6$ in EC:DEC, 1:1) reference electrolyte.

4.3.2 Electrochemical Performance

As seen above, cycling below room temperature can lead to rapid capacity fading due to large overpotentials limiting the capacity. As seen in Fig. 25, switching from an electrolyte containing EC to 1 M $LiPF_6$ dissolved in PC:DMC (50:50) allows stable cycling and coulombic efficiency at -9 °C, showing that these effects are electrolyte dependent.

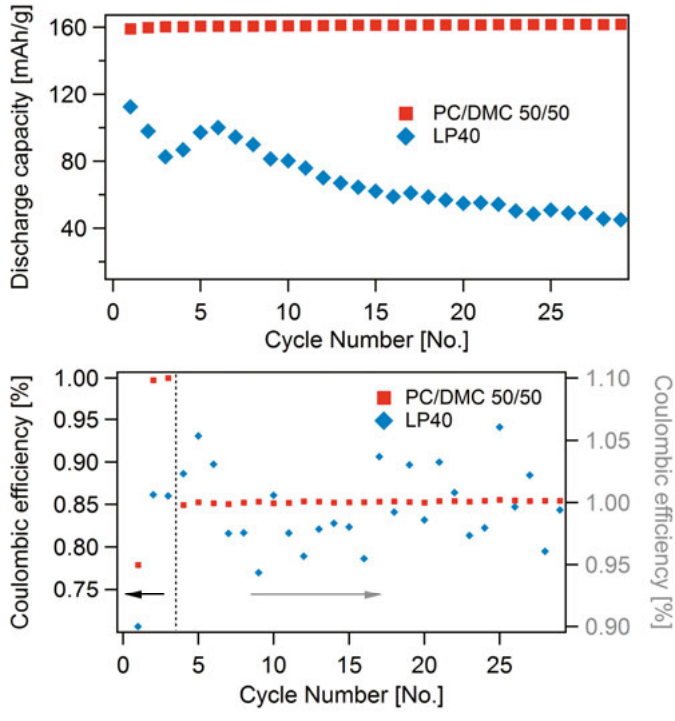

Figure 25. Cycling of NMC 622 vs. LTO between 1.45 V and 2.95 V: top) discharge capacity vs. cycle number, bottom) coulombic efficiency vs. cycle number.

To evaluate the electrolyte stability at high potentials, a cycling protocol containing pauses was performed. The cells were cycled with constant current constant voltage (CC-CV) charging and constant current (CC) discharge, with a pause (OCV period) inserted after some of the CC-CV charging steps; see Fig. 26. The capacity lost during the discharge following the pause was compared with the average of the discharge capacities of the previous and the following cycle. It is then seen that the PC containing electrolyte performs similarly to the EC containing electrolyte, having a smaller capacity loss than the electrolyte only containing DMC. This indicates that the presence of EC and PC leads to fewer side reactions, likely due to formation of a stabilized electrode interface preventing further electrolyte degradation.

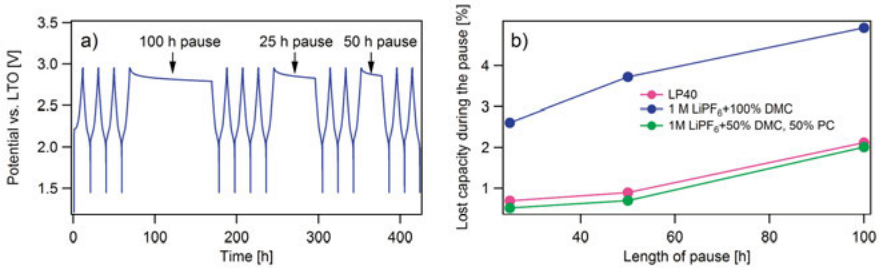

Figure 26. Cycling procedure applying a pause at 2.95 V: a) schematic representation of the cycling procedure, b) capacity lost in side reactions as a function of the pause length.

4.3.3 Electrode Surface Characterization

The electrodes were characterized with XPS to explore the degradation products formed on the electrodes. Fig. 27 shows the O 1s and C 1s core level spectra of the NMC electrodes. From the higher intensity of the metal-oxygen feature at 529 eV in the O 1s spectra of the electrolytes not containing PC, it is shown that the PC degrades on the electrode and forms a thicker surface layer. The degradation of PC at the electrode surface is also seen in the O 1s spectra from the higher intensity between 531 and 534 eV, coming from organic species, and in the C 1s spectra as the larger contribution at 288.8 eV correspond to C=O and/or O=C-O groups.[105,106] The reference electrolyte containing EC has a larger peak at ~290 eV corresponding to carbonates, showing that the EC degrades and forms a surface film on NMC.

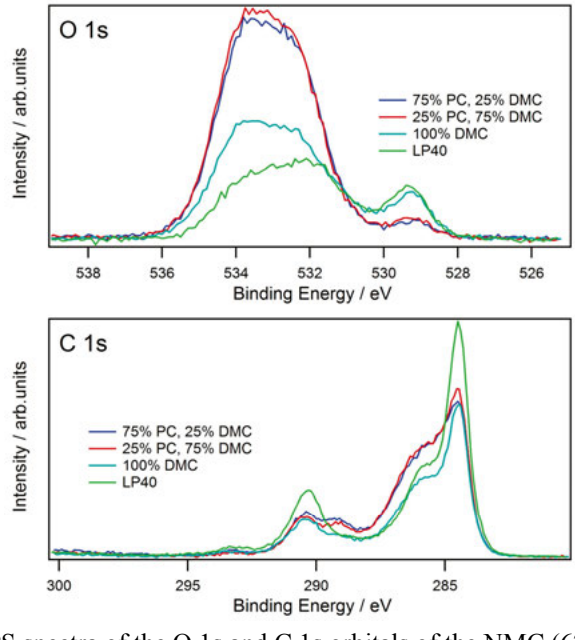

Figure 27. XPS spectra of the O 1s and C 1s orbitals of the NMC (622) electrodes.

The LTO electrodes were also analyzed with XPS. Fig. 28 shows the C 1s, O 1s, F 1s, P 2p and Ti 2p core levels. From the high intensity of the peak at 283.9 eV in the C 1s spectrum and of the metal-oxygen peak in the O 1s spectrum, it is seen that the surface layer is the thinnest in the cell cycled with LP40. This suggests that EC will react with the LTO electrode, making the surface stable and preventing further electrolyte degradation. Comparing the PC containing electrolytes with LP40, it is seen that the electrolytes have similar peaks around 287 eV and 290 eV corresponding to -O-C-O and carbonates, respectively. At about 285 eV the PC containing electrolytes have higher intensity, indicating formation of more hydrocarbons.

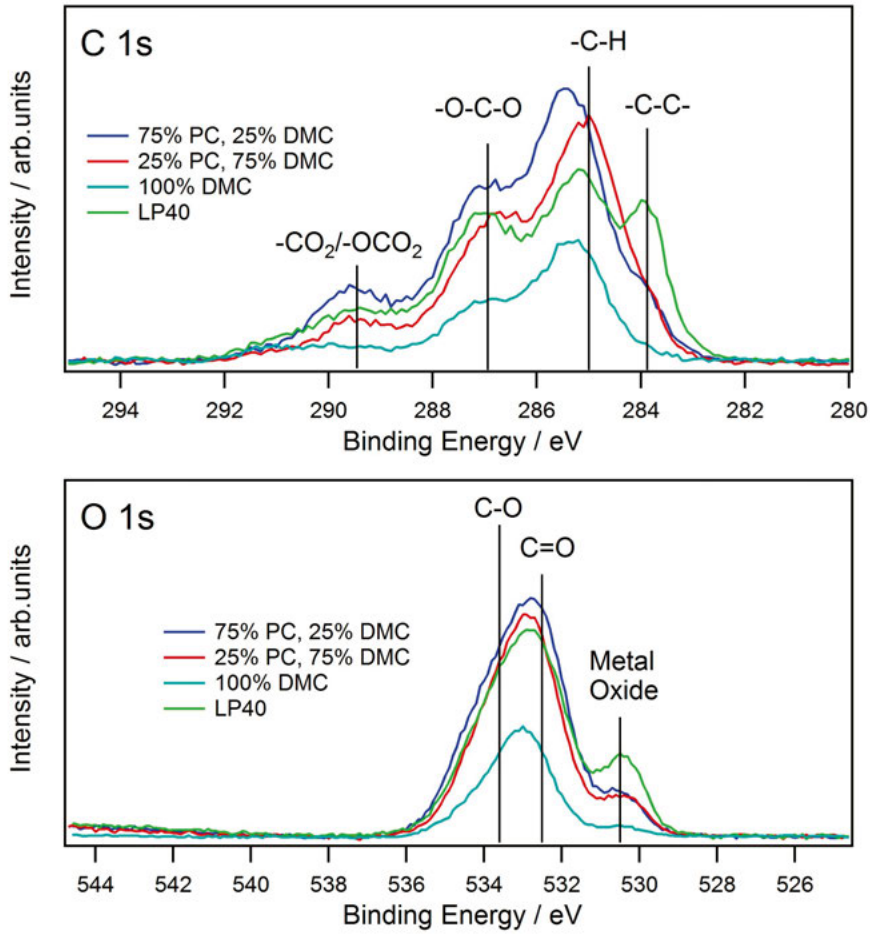

Figure 28. XPS spectra of the C 1s, O 1s, F 1s, P 2p and Ti 2p orbitals of the LTO electrodes.

Since PC-containing electrolytes showed good ionic conductivity and low temperature cycling performance, but PC degraded at both electrodes in LTO-

NMC cells, this indicates that the electrodes either should be stabilized somehow, or that a different solvent or cosolvent should be used to achieve a longer cycle life. Consequently, sulfolane was investigated as it is known to be stable towards oxidation.[29] Additionally, according to molecular dynamics simulations, a mixture of sulfolane with DMC should be more stable towards higher potentials than pure DMC.[107]

The degradation of EC at high potentials were investigated by XPS. In Fig. 29, the O 1s spectra of NMC electrodes charged to 5 V and 6 V with EC-free electrolytes as well as LP40 reference electrolyte are shown. It can be seen that the peak at 532.5 eV has much higher intensity in the samples cycled with the LP40, showing that EC breaks down at these potentials and forms a surface layer on the electrodes. The peak is wide, indicating that the EC will break down into various organic species. EC-free electrolytes thus seem more stable at higher potentials.

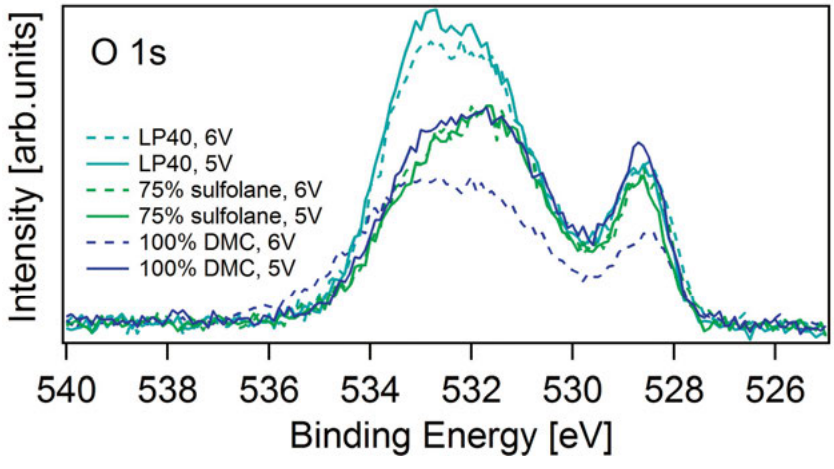

Figure 29. O 1s spectra of NMC-Li cells cycled to 5 and 6 V using different electrolytes.

4.3.4 Electrolyte Conductivity and Stability

Sulfolane has drawbacks, however, preventing it from being used in conventional electrolytes. Primarily, it has a high melting point of 28 °C[33] and also high viscosity. On the other hand, despite the high viscosity a mixture of DMC with sulfolane achieved higher conductivity than pure DMC, similar to the LP40 reference electrolyte; see Fig. 30.

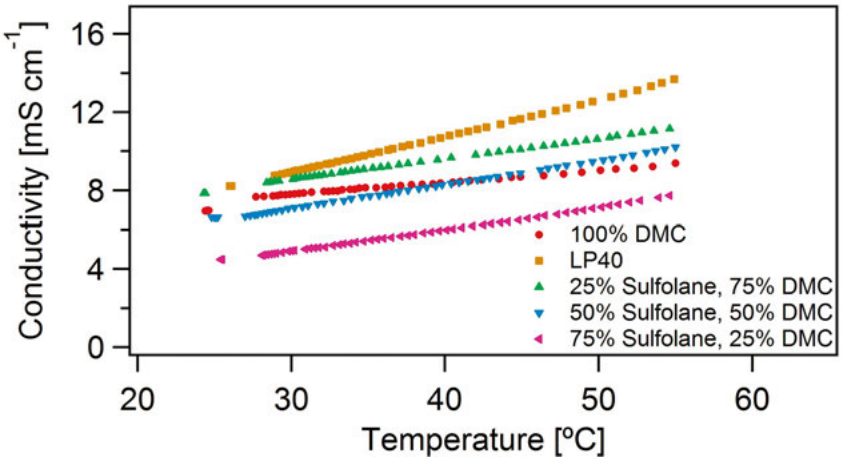

Figure 30. Ionic conductivity measured at different temperatures for electrolytes containing 1 M $LiPF_6$ in different ratios of sulfolane and DMC as well as LP40 reference electrolyte.

The electrochemical stability towards electrolyte oxidation was measured by Linear Sweep Voltammetry (LSV). It was found to be similar for all electrolytes, showing degradation above about 4.5 V; see Fig. 31. It has been shown with molecular dynamic simulations that the sulfolane will adsorb stronger to the positive electrode than the DMC, thereby increasing the distance between the electrode and the DMC.[107] The DMC molecules in a sulfolane based electrolyte are therefore likely to experience a lower electrochemical potential, and consequently less likely to be oxidized than DMC in a different electrolyte.[107] This phenomenon, however, does not seem to significantly affect the oxidation potential of the DMC in the mixtures with sulfolane investigated here, indicating that the sulfolane concentration must be high in order to increase the oxidation stability.

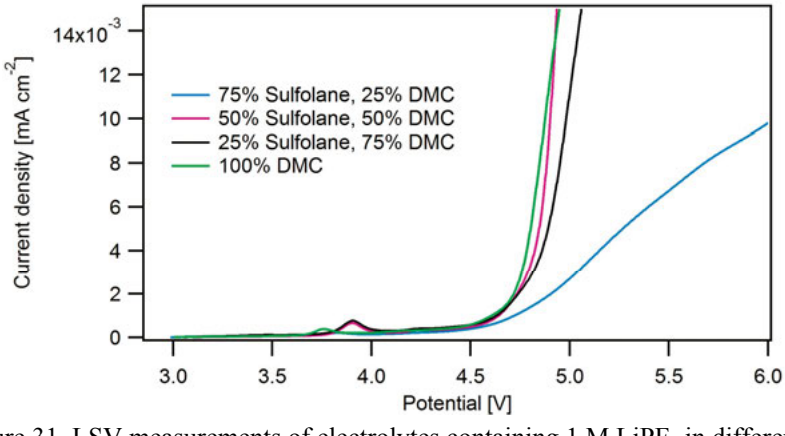

Figure 31. LSV measurements of electrolytes containing 1 M $LiPF_6$ in different ratios of sulfolane and DMC as well as LP40 reference electrolyte.

4.3.5 Surface Layer Formation in Sulfolane Based Electrolytes

Fig. 32 shows the C 1s, O 1s and Ti 2p core levels of the LTO electrodes after cycling 100 cycles using different ratios of sulfolane in the electrolytes. Both of the electrolytes containing sulfolane have a larger intensity than electrolytes containing pure DMC at 284.1 eV in the C 1s spectra, 530.4 eV in the O 1s spectra and 459 eV in the Ti 2p spectra corresponding to carbon black, oxygen in the LTO and titanium in the LTO, respectively. The high intensity of these compounds present in the bulk show that the surface layer is much thinner when sulfolane is present in the electrolyte as compared to pure DMC. In this context, it is interesting that the LP40 electrolyte forms a thinner surface layer than the pure DMC electrolyte; see Fig. 28. The surface layer for LP40 is still not as thin as what is observed for the sulfolane containing electrolytes. If compared with cycling data, a thin surface layer seems beneficial for the capacity retention.

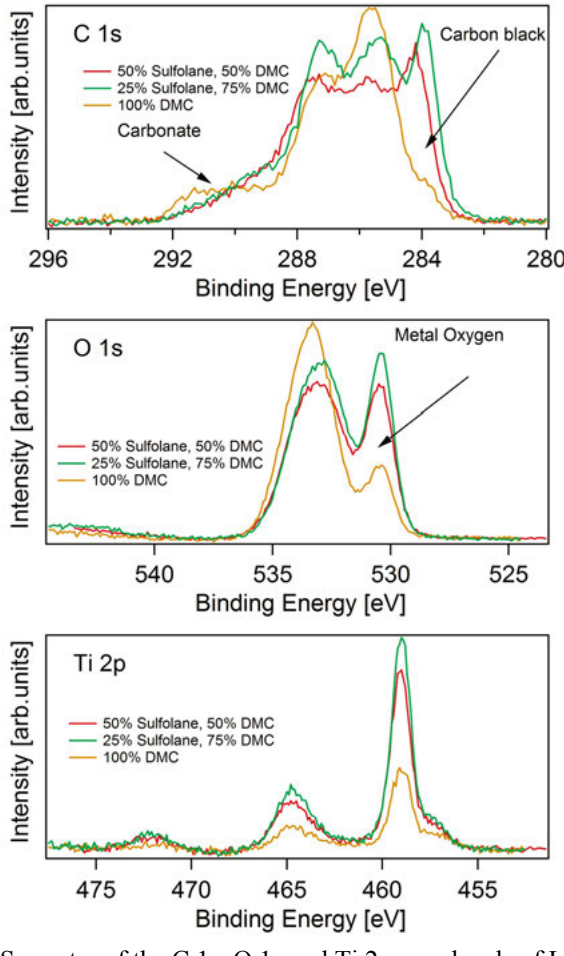

Figure 32. XPS spectra of the C 1s, O 1s and Ti 2p core levels of LTO electrodes after cycling.

4.4 Investigation of Commercial Cells

This section describes the effect of temperature and state of charge (SOC) interval on capacity fading of commercial NMC/LMO vs. graphite cells. The aim was to analyze the ageing mechanisms limiting the capacity after long term cycling. The results based on SOC-level cycling that are presented in this section are based on Paper V.

4.4.1 Cycling Results of the Cells

In Fig. 33, the capacity retention of four cells cycled at different temperatures and in different SOC intervals are shown. Two of the cells are cycled at 25 °C and 45 °C in the range of 0-90 % SOC, and the other two cells are cycled in the range of 10-20 % SOC and 60-70% SOC at 45 °C. It should be noted that all cells are cycled for different amount of time, which is also likely affecting their ageing. The cells were stopped when reaching about 80 % of the initial SOC value, but the cell cycled at 45 °C in the range of 0-90 % SOC reached 72 % of the initial SOC value and the cell cycled in the range of 10-20 % SOC at 45 °C reached 92 % of the initial SOC value. Since the cells are cycled both to different SOC levels and for different number of cycles, it is difficult to make any firm conclusions through straightforward comparisons between the cells, though.

It is seen that the capacity fading in the cell cycled at 45 °C for 0-90 % SOC is the most rapid out of all cells. It is also seen that the capacity fading is worse in the cell cycled between 60 and 70 % SOC than the cell cycled between 10 and 20 % SOC.

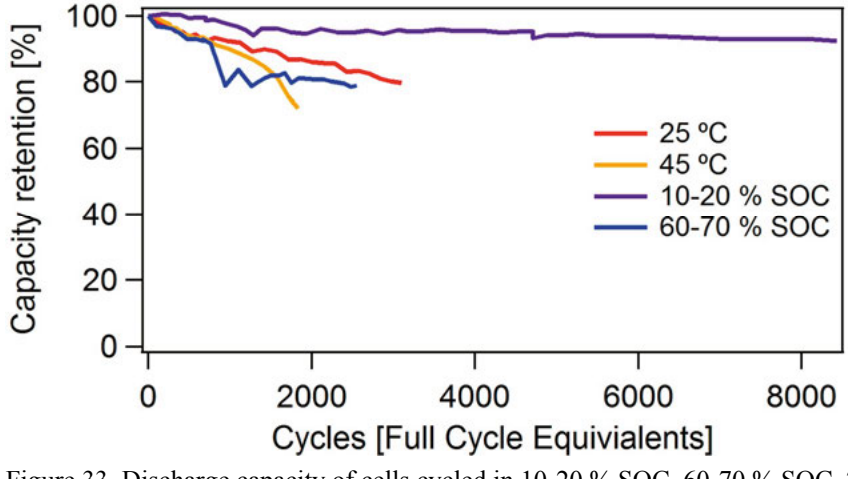

Figure 33. Discharge capacity of cells cycled in 10-20 % SOC, 60-70 % SOC, 25 °C and 45 °C. Cycling performed by E. Wikner, Chalmers University of Technology.

4.4.2 Electrochemical Performance of Cycled Electrodes

Fig. 34 shows the incremental capacity plots of commercial NMC/LMO electrodes cut out from the cells before and after cycling, and reassembled into lab-scale cells with lithium as negative electrode. It is seen that the capacity of the NMC/LMO electrodes (corresponding to the area of the incremental capacity plot) is smaller for the cycled electrodes than the uncycled electrodes. The result is similar both for cycling at different temperatures and different SOC intervals. The cycling was performed at a low current of 0.1 mA/cm^2, making contribution from resistive effects small. Since resistive effects should have negligible impact on the performance of the NMC/LMO electrodes, the decreased capacity must be explained by permanent damage to the electrode material, i.e. loss of active material (loss of contact between particles, material degradation etc.). In the incremental capacity plots, the peak at 3.74 V corresponds to the NMC particles and the peaks at 4.00 and 4.14 V correspond to lithiation of the LMO particles. Since it can be seen that the major capacity loss is caused by the peak at 3.74 V, it can be concluded that it is the NMC particles that are the cause for loss of active material during cycling.

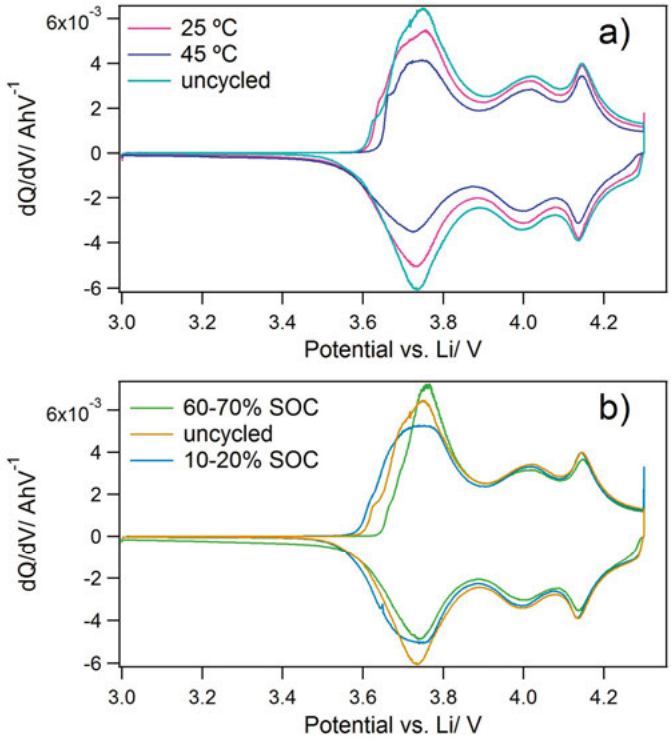

Figure 34. Incremental capacity plots of NMC/LMO electrodes cycled vs. lithium. a) NMC/LMO electrodes previously cycled at 25 °C, 45 °C and uncycled electrode. b) NMC/LMO electrodes previously cycled between 10 and 20 % SOC, 60 and 70 % SOC and uncycled electrode.

In Table 2, the discharge capacity of both the lab-scale NMC/LMO vs. Li cells and graphite vs. Li cells are shown at two different C-rates. At the current of 0.1 mA/cm^2, less capacity loss is observed in the graphite vs. Li cells than the NMC/LMO vs. Li cells, indicating less loss of active material in the graphite electrodes. After cycling at higher current, however, the discharge capacity of the graphite vs. Li cells is far less than the NMC/LMO vs. Li cells. This means that during cycling at a higher C-rate – closer to the rate used during the ageing test – the graphite electrodes will limit the capacity in the cells. The graphite electrodes are therefore limited by the resistance during cycling.

Table 2. Discharge capacity (mAh/cm^2) of graphite vs. lithium and NMC/LMO vs. lithium at different C-rates during the third cycle.

	Graphite vs. Li					**NMC/LMO vs. Li**				
	Uncycled	25 °C	60-70% SOC	10-20% SOC	45 °C	Uncycled	25 °C	60-70% SOC	10-20% SOC	45 °C
Discharge capacity at 0.1 mA/cm^2	0.73	0.71	0.72	0.72	0.65	0.72	0.65	0.66	0.70	0.52
Discharge capacity at 3.0 mA/cm^2	0.29	0.31	0.19	0.29	0.22	0.61	0.51	0.45	0.60	0.33

4.4.3 The Electrode Surfaces and Electrolyte Decomposition

Fig. 35 shows the P 2p spectra and the F 1s spectra of the graphite electrodes cycled at different temperatures. In the P 2p spectra, a peak at 136.8 eV (corresponding to P-F containing SEI species) is present in all samples. In the cell cycled at 45 °C, however, a small peak at 134.3 eV is also present. For the electrode cycled at 45 °C, the relative contribution from the P-O species is far larger than that observed at the electrode cycled at 25 °C. The observed phosphorus compounds should be caused by degradation products of the $LiPF_6$ salt. $LiPF_6$ salt degradation in organic electrolytes at elevated temperatures have previously been shown, where formation of HF take place.[61] HF is known to cause various side reactions including reaction with electrode particles[108,43] or the surface films on the electrodes[109,47] leading to shorter cycle life. The increased presence of $LiPF_6$ salt degradation products detected could therefore indicate formation of more HF leading to a shorter cycle life.

The peaks observed in the F 1s spectra can also be caused by degradation products of the $LiPF_6$ salt. The peak at 687 eV corresponds to P-F compounds and the peak at 685 eV corresponds to LiF. At 45 °C, it is seen that the relative contribution of LiF is larger than in the uncycled electrode and the electrode cycled at 25 °C.

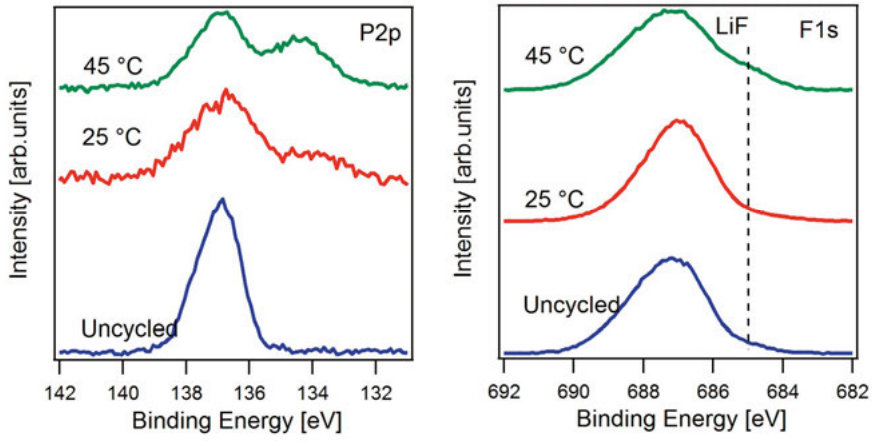

Figure 35. XPS measurements of the P 2p and the F 1s spectra of graphite electrodes after cycling at different temperatures.

Fig. 36 shows the core level spectra of graphite electrodes cycled in 10-20 % SOC, 60-70 % SOC and also uncycled electrodes. The manganese spectra are intensity normalized against the carbon intensity of the corresponding sample, allowing rough comparisons of intensity between different spectra. In the Mn 2p spectra, a large intensity contribution is observed in the cell cycled in the 60-70 % SOC interval, whereas the intensity is weak in the cell cycled at 10-20 % SOC and barely visible in the uncycled cell. This indicates dissolution of manganese from the NMC/LMO electrode and subsequent transportation towards the graphite electrode. The large differences in manganese intensity therefore indicate that manganese dissolution is more severe in the 60-70 % SOC interval than the 10-20 % SOC interval. It has previously been found that manganese dissolution is more severe at higher potentials,[41] corresponding well with the observation of more manganese dissolution in the 60-70 % SOC. Manganese dissolution has previously been attributed to cause increased resistance in the graphite SEI layer, likely caused by reaction products between the manganese and SEI components hindering the Li-ion diffusion.[41]

In the F 1s spectra a peak corresponding to P-F compounds in the SEI layer is observed as well as a peak corresponding to LiF. The spectra are obtained using two different photon energies, making it possible to distinguish where in the SEI layer the species are found. In both cycled electrodes a higher intensity of LiF is obtained using 6795 eV as photon energy, indicating a larger concentration of LiF in the inner part of the SEI layer than the outer part. In

the uncycled sample, however, no major differences are observed, thereby indicating a homogeneous distribution of species through the surface layer.

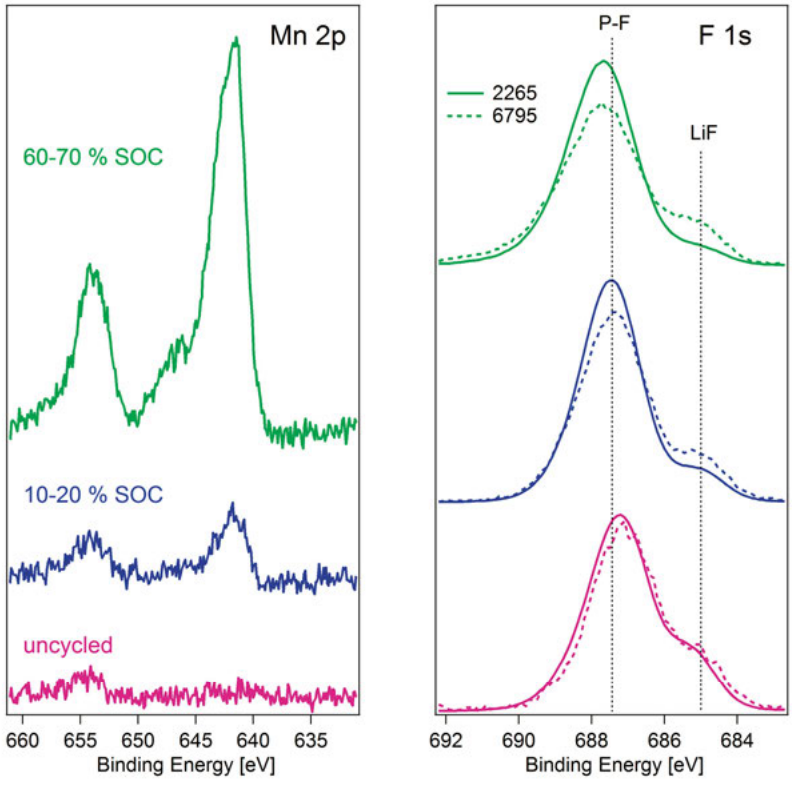

Figure 36. Synchrotron based measurements of the Mn 2p and the F 1s spectra of graphite electrodes after cycling in different SOC intervals. Solid lines corresponding to measurements at 2265 eV and dashed lines corresponding to measurements at 6795 eV.

4.4.4 Discussion Regarding Electrochemical Performance and Surface Chemistry

From the cycling results, it was found that the graphite electrodes limited the capacity of the cells at higher C-rates both for cells cycled at different temperatures and in different SOC intervals. Since the graphite electrodes only had minor capacity fading at a slow C-rate, the capacity loss is attributed to resistive limitations of the electrode. This correlates well with the XPS results, where we see relatively higher concentrations of $LiPF_6$ degradation compounds during cycling at 45 °C than during cycling at 25 °C or in the uncycled cells. However, in cells cycled in different SOC intervals, the largest difference is instead the amount of manganese dissolution, where it is far higher in the cell cycled at 60-70 % SOC than the cell cycled at 10-20 % SOC or in the uncycled cell.

5. Conclusions

Ageing of batteries, primarily shown as capacity fade, forms the context of this thesis work. It presents investigations of surface chemistry and electrochemical performance of LIB cells in both commercial and lab scale systems.

It is shown that the capacity retention in cells containing NMC as positive electrode is to a large extent influenced by the negative electrode material, where lithium foil has a poor performance as compared to graphite and LTO. The poor performance in NMC-Li cells seems to be caused by excessive electrolyte degradation at the lithium foil, leading to diffusion of degradation products from the lithium foil towards the NMC electrode. XPS studies showed that the surface layer on NMC electrodes mainly consists of organic compounds after cycling vs. lithium foil, as opposed to graphite and especially LTO where the inorganic compounds have a larger presence. In NMC-Li cells, it is also shown that the buildup of surface layers occurs gradually during the battery cycling, as opposed to the ideal case where the surface layer formation process is finished after the first few cycles. The poor capacity retention caused by gradual electrolyte degradation in NMC-Li cells is one of the obstacles for the use of lithium in commercial cells, where instead a less reactive electrode material should be used to achieve long cycle life.

These studies also highlight the importance of cycling the cells within the right temperature interval to decrease ageing, avoiding both cold and warm environments. At high temperatures, continuous side reactions took place at the LTO throughout the cycling, causing a loss of active lithium and capacity loss due to a slippage of the electrode's potential window. At 30 °C, less side reactions took place at the LTO. Moreover, the initial electrolyte reduction at the LTO electrode stabilized the NMC electrode, leading to a higher capacity retention. At subzero temperatures the cycling performance was poor, mainly caused by the high cell resistance.

It could, however, be seen that low temperature cycling performance could be improved by changing the electrolyte. By exchanging the EC in the electrolyte to PC, cycling was performed without capacity fading. But even though it is beneficial if cells can operate at low temperatures, the cells must generally be able to cycle at higher temperatures too. Unfortunately, PC participated in side reactions at both of the electrodes during cycling at 30 °C, contributing to thicker surface layers and capacity losses. This illustrates the difficulties in finding an electrolyte that can operate in both sub-zero and ambient environments.

The degradation of EC at high potentials was also found to form surface films on the positive electrode. This supports that exchanging EC for a different, more stable, solvent should be beneficial. Replacing EC with sulfolane, however, led to similar capacity fading during cycling. Sulfolane still performed better than pure DMC, which is another possibility for high voltage cells where the conventional EC containing electrolytes might be replaced. Both EC and sulfolane based electrolytes had thinner surface layers than the pure DMC electrolytes – that are supposed to be stable – indicating that these electrolytes either are more stable or form more stable surface layers and prevent further degradation and ageing.

In commercial cells, it was seen that cycling at lower temperature (25 °C) and lower SOC intervals prevent cell degradation. Furthermore, it was shown that the NMC/LMO electrodes undergo more loss of active material than the graphite electrodes, independent of temperatures or SOC intervals investigated. Especially NMC particles degrade to a larger extent as compared to LMO particles.

Increasing the temperature from 25 °C to 45 °C will cause an increase of $LiPF_6$ salt degradation on the graphite electrodes, indicating that this could be one of the reasons for the poor capacity retention at higher temperatures. Avoiding elevated temperatures during cycling is therefore crucial for keeping a long cycle life, at least for this cell chemistry. If the SOC interval is changed from 10-20 % SOC to 60-70 % SOC, an increase of manganese is observed on the graphite electrode, indicating that manganese dissolution is an important factor at high SOC intervals, leading to worse SEI layers. The increased manganese dissolution at higher SOC intervals seems to be the cause of the more rapid capacity fading observed. For applications where cycling is performed in a limited SOC interval, choosing a low SOC interval will decrease the effects of the severe ageing mechanisms, thereby allowing a longer cycle life.

These studies have stressed how the interplay between surface chemistry and electrochemical performance in LIB cells affect ageing using NMC, graphite, LTO and lithium electrodes. Ageing of batteries is a sensitive and complex phenomenon to study, because there are several factors contributing, each being detrimental for the cycle life. From these above studies, it was found how the capacity retention is reduced by electrolyte degradation at either the negative or the positive electrode, increased cell resistance, and manganese dissolution. Despite these many issues, there nevertheless exist possibilities to circumvent rapid degradation. Especially the choice of cell chemistry is of large importance, where reactive electrodes and electrolytes should be avoided. During normal operating conditions, a combination of many of the common LIB materials are suitable (except lithium foil which is too reactive). For instance, using LTO was even found to be stabilizing the side reactions at the NMC electrode. If the application on the other hand requires low temperatures, the standard EC containing electrolyte should be exchanged for

a solvent with lower freezing point such as PC, which possesses many of EC's beneficial properties. For applications requiring a very long cycle life, it is preferable to cycle the cells in a low SOC interval, so that manganese dissolution can be avoided. In applications where cells with a high energy density are required and the cells therefore have to be charged to high potentials, it is beneficial to use electrolytes which do not degrade, e.g. sulfolane-based. Thus, using the right cell chemistry for the right cycling condition is essential for reaching a long cycle life and avoiding ageing.

6. Sammanfattning på svenska

Antalet litium-jonbatterier har under de senaste åren ökat i många tillämpningar. Inte minst har detta gällt portabel elektronik, men även i större produkter som elektriska fordon. De många tillämpningarna ställer olika krav på batterierna. I portabel elektronik så har storlek och vikt stor betydelse medan pris och livstid inte har samma betydelse – batterierna behöver ändå inte hålla så många år. I elektriska fordon däremot så har pris och livstid mycket större betydelse. Det handlar om batterier som ofta väger mer än hundra kilo, och som därmed innehåller en stor mängd dyra och sällsynta material, samt att man vill använda en bil under mycket längre tid än en bärbar dator eller mobiltelefon. Detta gör *åldrandet* av batteriet centralt.

Mänskligheten har sedan urminnes tider fascinerats och skrämts av åldrandet. Detta gäller så väl oss själva som det som omger oss: vi målar, opererar, renoverar, förbättrar och förstärker både oss själva, byggnader och saker. I princip åldras alla material, och materialen i batterier utgör inget undantag. Litium-jonbatterier degraderar sakta medan de används, men även när de inte används. Degraderingsprocesserna beror på vad det finns för material i cellerna samt under vilka betingelser batterierna används. I ett vanligt litium-jonbatteri finns det två elektroder som har en stor potentialskillnad mellan varandra, t.ex. grafit och litiumnickelmangankoboltoxid (NMC) är ofta använda. Det är den stora potentialskillnaden mellan elektroderna gör så att det är svårt för kemiska föreningar att inte degradera i kemiska sidoreaktioner. Det övergripande syftet med forskningen i denna avhandling är att undersöka vilka degraderingsprocesser som sker i NMC-baserade litium-jonbatterier beroende på hur cellen används och vilka material som ingår i cellen.

Hur olika elektroder påverkar livslängden i NMC-baserade celler undersöktes då NMC cyklades mot grafit, litiumtitanat samt litiumfolie i olika batterier. Det visade sig att kapacitetsförlusten var låg i celler där NMC cyklades mot litiumtitanat och grafit, medan den var hög i celler där NMC cyklats mot litiumfolie. Analys av den kemiska sammansättningen m.h.a. röntgenfotoelektronspektroskopi av NMC-elektroderna visade att det fanns mer organiska nedbrytningsprodukter i cellen med NMC-litium, och att mängden nedbrytningsprodukter ökar med tid som cellen har cyklats. Detta stämmer också väl med hur överpotentialen ökar med tiden i denna typ av celler. Den ökade mängden organiska nedbrytningsprodukter på NMC-elektroden som observerades i NMC-litiumcellen visar att degradering av elektrolyten sker vid litium-

folien, medan degraderingsprodukterna därefter diffunderar över till NMC-elektroden.

Även val av elektrolyt undersöktes för att minska åldring i celler cyklade till höga potentialer. För att elektrolyten skulle bli mer stabil byttes etylenkarbonaten (EC) – vilken visat sig vara instabil vid höga potentialer – ut mot propylenkarbonat (PC). Dessa elektrolyter har hög konduktivitet, vilket är bra om cellen ska laddas snabbt. Tyvärr visade det sig att även PC var förhållandevis instabil vid höga potentialer och reagerade på elektroderna så att tjocka ytlager bildades. Därför undersöktes även ett annat lösningsmedel som gjort sig känt för att vara stabil vid dessa betingelser. Detta lösningsmedel utgjordes av sulfolanmolekyler, och verkade bra eftersom celler som laddats upp till 5 V inte skapade något tjockt lager av degraderingsprodukter. Även efter flertalet upp- och urladdningar av batterier så blev ytlagret betydligt tunnare med sulfolan i elektrolyten, vilket tyder på att den inte degraderar så mycket, och därmed inte åldras lika snabbt.

Förutom olika cellkemier så undersöktes även hur temperatur påverkar cykling av celler. Vid 30 °C kunde cellerna cykla utan att åldras mycket. Däremot vid både -10 °C och 55 °C åldrades cellerna snabbt. Det visade sig att vid 30 °C så stabiliserade reaktionerna vid litiumtitanaten (den negativa elektroden) NMC-elektroden, så att cellen kunde cykla utan att åldras. Vid 55 °C var inte stabiliseringen tillräckligt bra, vilket fick elektrolyten att reagera vid LTO elektroden. Vid -10 °C var å andra sidan resistansen så stor att all kapacitet inte kunde användas. För att cykla vid låga temperaturer är val av elektrolyt viktigt, och då är lösningsmedelsmolekylernas smältpunkt av stor betydelse. Därför användes även elektrolyt som innehöll propylenkarbonat (som har en låg smältpunkt) i stället för etylenkarbonat, vilket fungerade väl utan att cellen åldrades.

Slutligen undersöktes även kommersiella celler i denna avhandling. Cellerna hade laddats och urladdats i begränsande intervall eller använts vid olika temperaturer. Det visade sig att celler som laddats upp och ur mellan 10 till 20 procent av batteriets kapacitet hade mycket mindre kapacitetsförluster än celler som laddats upp och ur mellan 60 till 70 procent. Efter att batterierna cyklats klart plockades de isär för att sedan åter sättas ihop till celler där elektrodernas individuella kapaciteter kunde bestämmas. Det visade sig att den positiva elektroden hade degraderats mer än den negativa elektroden, men att det är den negativa elektroden som kommer att begränsa kapaciteten av cellen vid snabba upp och urladdningar. Röntgenfotoelektronspektrometrimätningar kunde visa att det sannolikt är utlösning av mangan ur den positiva elektroden tillsammans med ett något tjockare lager av elektrolytdegraderingsprodukter som orsakar den korta livslängden då cellen cyklats mellan 60 och 70 % av dess kapacitet.

För att undvika snabbt åldrande är det därför fördelaktigt att inte förvara cellerna varmt, eller att använda dem utomhus på vintern. Dessutom är det bättre att ladda batterierna ofta men då att undvika att ladda dem fullt. Genom

att anpassa materialen i cellen och tillämpa ett snällt användande av batterierna så är det möjligt att använda dem i flera år utan att de behöver bytas ut.

7. Acknowledgements

First of all I would like to thank my supervisors Kristina Edström, Daniel Brandell and Reza Younesi. Thank you for allowing me doing research so freely, making me enjoy these years! I would like to thank Reza for a lot of support I have received, Daniel for his encouragement and for helping me whenever I needed and to Kristina for starting my way as a PhD-student, setting me on the right path.

I would like to thank Mara Göttlinger for helping me performing lab work and nice discussions.

I am happy for all the help I have received from all other people who have been coauthors on papers and manuscripts: Chao Xu, Evelina Wikner, Maria Hahlin, Andy Naylor, Will Brant and Tim Nordh.

Thank you everyone in the *Aging mechanisms and how to prolong battery life in vehicles and stationary applications* (APL) project, the project funding this work through the Swedish Energy Agency. I would especially like to thank Evelina who have helped me during lots of phone calls and email conversations and for making the conferences more fun.

Sincere thanks to Maria, Julia Maibach, Tim and Reza for introducing me to XPS and helping me make sense of the results. Also many thanks to everybody else participating in the beam times: Burak Aktekin, Ida Källquist, Fabian Jeschull, Kazuhiro Hikima, Chao, Andy and Fredrik Lindgren.

I would like to thank Henrik Eriksson, Rickard Eriksson and Long for keeping the lab-equipment working.

I would like to thank Sebastian Öhman for making my last years in the office nicer. I also have to thank Mahsa Ebadi, Ruijun Pan, Chenjuan Liu and Burak for many enjoyable conversations. Thank you all people at the coffee table for all nice discussions during the years.

Thanks to all people working in the battery group and other people who have worked with me: Mario, Matt, Erik, Haidong, Ming, Stéven, Torbjörn, David, Andreas, Le Anh, Jonas, Yonas, Habtom, Hohyoun, Solveig, Viktor, Alina, Julia, Shruti, Fernanda, Charlotte, Charifa, Anti, Ashok, Tatiana, Will, Ronnie, Ocean, Linus, Kristina, Sarmad, Shuainan, Johan, Siham, Paulius, Therese, Andoria, Guiomar, Marco, Yu-Chuan, Christofer, Ida, Isabell, Yutaro, Dennis, Adam for all discussions.

Also, I would like to thank all people who have managed to read this far!

Finally, I would like to thank my parents and brother for encouraging and inspiring me.

8. References

(1) Vetter, J.; Novák, P.; Wagner, M. R.; Veit, C.; Möller, K. C.; Besenhard, J. O.; Winter, M.; Wohlfahrt-Mehrens, M.; Vogler, C.; Hammouche, A. Ageing Mechanisms in Lithium-Ion Batteries. *J. Power Sources* **2005**, *147*, 269–281.

(2) Mukhopadhyay, A.; Sheldon, B. W. Deformation and Stress in Electrode Materials for Li-Ion Batteries. *Prog. Mater. Sci.* **2014**, *63* (February), 58–116.

(3) Arora, P.; White, R. E.; Doyle, M. Capacity Fade Mechanisms and Side Reactions in Lithium-Ion Batteries. *J. Electrochem. Soc.* **1998**, *145* (10), 3647–3667.

(4) Zhang, W. J. Structure and Performance of LiFePO4 Cathode Materials: A Review. *J. Power Sources* **2011**, *196* (6), 2962–2970.

(5) Yuan, L.-X.; Wang, Z.-H.; Zhang, W.-X.; Hu, X.-L.; Chen, J.-T.; Huang, Y.-H.; Goodenough, J. B. Development and Challenges of LiFePO $_4$ Cathode Material for Lithium-Ion Batteries. *Energy Environ. Sci.* **2011**, *4* (2), 269–284.

(6) Wu, X. L.; Jiang, L. Y.; Cao, F. F.; Guo, Y. G.; Wan, L. J. LiFePO4 Nanoparticles Embedded in a Nanoporous Carbon Matrix: Superior Cathode Material for Electrochemical Energy-Storage Devices. *Adv. Mater.* **2009**, *21* (25–26), 2710–2714.

(7) Song, J.; Sun, B.; Liu, H.; Ma, Z.; Chen, Z.; Shao, G.; Wang, G. Enhancement of the Rate Capability of LiFePO4 by a New Highly Graphitic Carbon-Coating Method. *ACS Appl. Mater. Interfaces* **2016**, *8* (24), 15225–15231.

(8) Nan, C.; Lu, J.; Li, L.; Li, L.; Peng, Q.; Li, Y. Size and Shape Control of LiFePO4 Nanocrystals for Better Lithium Ion Battery Cathode Materials. *Nano Res.* **2013**, *6* (7), 469–477.

(9) Xu, B.; Qian, D.; Wang, Z.; Meng, Y. S. Recent Progress in Cathode Materials Research for Advanced Lithium Ion Batteries. *Mater. Sci. Eng. R Reports* **2012**, *73* (5–6), 51–65.

(10) Aurbach, D.; Levi, M. .; Gamulski, K.; Markovsky, B.; Salitra, G.; Levi, E.; Heider, U.; Heider, L.; Oesten, R. Capacity Fading of LixMn2O4 Spinel Electrodes Studied by XRD and Electroanalytical Techniques. *J. Power Sources* **1999**, *81–82*, 472–479.

(11) Nitta, N.; Wu, F.; Lee, J. T.; Yushin, G. Li-Ion Battery Materials: Present and Future. *Mater. Today* **2015**, *18* (5), 252–264.

(12) Aurbach, D.; Teller, H.; Koltypin, M.; Levi, E. On the Behavior of Different Types of Graphite Anodes. *J. Power Sources* **2003**, *119–121*, 2–7.

(13) Shu, Z. X.; Mcmillan, R. S.; Murray, J. J. Electrochemical Intercalation of Lithium into Graphite. *J. Electrochem. Soc.* **1993**, *140* (4), 922.

(14) Zane, D.; Antonini, A.; Pasquali, M. A Morphological Study of SEI Film on Graphite Electrodes. *J. Power Sources* **2001**, *97–98*, 146–150.

(15) Verma, P.; Maire, P.; Novák, P. A Review of the Features and Analyses of the Solid Electrolyte Interphase in Li-Ion Batteries. *Electrochim. Acta* **2010**, *55*, 6332–6341.

(16) Cheng, X. B.; Zhang, R.; Zhao, C. Z.; Wei, F.; Zhang, J. G.; Zhang, Q. A Review of Solid Electrolyte Interphases on Lithium Metal Anode. *Adv. Sci.* **2015**, *3* (3), 1–20.
(17) Goriparti, S.; Miele, E.; De Angelis, F.; Di Fabrizio, E.; Proietti Zaccaria, R.; Capiglia, C. Review on Recent Progress of Nanostructured Anode Materials for Li-Ion Batteries. *J. Power Sources* **2014**, *257*, 421–443.
(18) Takeda, Y.; Yamamoto, O.; Imanishi, N. Lithium Dendrite Formation on a Lithium Metal Anode from Liquid, Polymer and Solid Electrolytes. *Electrochemistry* **2016**, *84* (4), 210–218.
(19) Schechter, A.; Aurbach, D.; Cohen, H. X-Ray Photoelectron Spectroscopy Study of Surface Films Formed on Li Electrodes Freshly Prepared in Alkyl Carbonate Solutions. *Langmuir* **1999**, *15* (9), 3334–3342.
(20) Aurbach, D.; Zinigrad, E.; Cohen, Y.; Teller, H. A Short Review of Failure Mechanisms of Lithium Metal and Lithiated Graphite Anodes in Liquid Electrolyte Solutions. *Solid State Ionics* **2002**, *148* (3–4), 405–416.
(21) Transactions, E. C. S.; Society, T. E. Performances Of Lithium-Ion Cells Constituted Of NMC // LTO Electrodes And Ionic Liquid Or Carbonates-Based Electrolytes L. Chancelier. **2014**, *61* (27), 69–77.
(22) Wu, K.; Yang, J.; Zhang, Y.; Wang, C.; Wang, D. Investigation on Li4Ti5O12 Batteries Developed for Hybrid Electric Vehicle. *J. Appl. Electrochem.* **2012**, *42* (12), 989–995.
(23) Sun, X.; Hegde, M.; Zhang, Y.; He, M.; Gu, L.; Wang, Y.; Shu, J.; Radovanovic, P. V.; Cui, B. Structure and Electrochemical Properties of Spinel Li4Ti5O12 Nanocomposites as Anode for Lithium-Ion Battery. *Int. J. Electrochem. Sci.* **2014**, *9* (4), 1583–1596.
(24) Chancelier, L.; Santini, C. C.; Gutel, T.; Mailley, S. Performances Of Lithium-Ion Cells Constituted Of NMC // LTO Electrodes And Ionic Liquid Or Carbonates-Based Electrolytes L. Chancelier. *ECS Electrochem. Lett.* **2014**, *61* (27), 69–77.
(25) Logan, E. R.; Tonita, E. M.; Gering, K. L.; Li, J.; Ma, X.; Beaulieu, L. Y.; Dahn, J. R. A Study of the Physical Properties of Li-Ion Battery Electrolytes Containing Esters. *J. Electrochem. Soc.* **2018**, *165* (2), A21–A30.
(26) Self, J.; Wood, B. M.; Rajput, N. N.; Persson, K. A. The Interplay between Salt Association and the Dielectric Properties of Low Permittivity Electrolytes: The Case of LiPF6 and LiAsF6 in Dimethyl Carbonate. *J. Phys. Chem. C* **2018**, *122* (4), 1990–1994.
(27) Borodin, O.; Olguin, M.; Ganesh, P.; Kent, P. R. C.; Allen, J. L.; Henderson, W. A. Competitive Lithium Solvation of Linear and Cyclic Carbonates from Quantum Chemistry. *Phys. Chem. Chem. Phys.* **2016**, *18* (1), 164–175.
(28) Kalhoff, J.; Eshetu, G. G.; Bresser, D.; Passerini, S. Safer Electrolytes for Lithium-Ion Batteries: State of the Art and Perspectives. *ChemSusChem* **2015**, *8* (13), 2154–2175.
(29) Li, S.; Li, B.; Xu, X.; Shi, X.; Zhao, Y.; Mao, L.; Cui, X. Electrochemical Performances of Two Kinds of Electrolytes Based on Lithium Bis(Oxalate)Borate and Sulfolane for Advanced Lithium Ion Batteries. *J. Power Sources* **2012**, *209*, 295–300.
(30) Ponrouch, A.; Marchante, E.; Courty, M.; Tarascon, J. M.; Palac??n, M. R. In Search of an Optimized Electrolyte for Na-Ion Batteries. *Energy Environ. Sci.* **2012**, *5* (9), 8572–8583.
(31) Tilstam, U. Sulfolane: A Versatile Dipolar Aprotic Solvent. *J. Power Sources* **2012**, *16* (7), 1273–1278.

(32) Wrodnigg, G. H.; Besenhard, J. O.; Winter, M. Cyclic and Acyclic Sulfites: New Solvents and Electrolyte Additives for Lithium Ion Batteries with Graphitic Anodes? *J. Power Sources* **2001**, *97–98*, 592–594.
(33) Della Monica, M.; Jannelli, L.; Lamanna, U. Physicochemical Properties of Sulfolane. *J. Phys. Chem.* **1968**, *72* (3), 1068–1071.
(34) Xie, Y.; Zou, H.; Xiang, H.; Xia, R.; Liang, D.; Shi, P.; Dai, S.; Wang, H. Enhancement on the Wettability of Lithium Battery Separator toward Nonaqueous Electrolytes. *J. Memb. Sci.* **2016**, *503*, 25–30.
(35) Liu, C.; Neale, Z. G.; Cao, G. Understanding Electrochemical Potentials of Cathode Materials in Rechargeable Batteries. *Mater. Today* **2016**, *19* (2), 109–123.
(36) Gauthier, M.; Carney, T. J.; Grimaud, A.; Giordano, L.; Pour, N.; Chang, H.-H.; Fenning, D. P.; Lux, S. F.; Paschos, O.; Bauer, C.; Maglia, F.; Lupart, S.; Lamp, P.; Shao-Horn, Y. The Electrode-Electrolyte Interface in Li-Ion Batteries: Current Understanding and New Insights. *J. Phys. Chem. Lett.* **2015**, acs.jpclett.5b01727.
(37) Kasnatscheew, J.; Streipert, B.; Röser, S.; Wagner, R.; Cekic Laskovic, I.; Winter, M. Determining Oxidative Stability of Battery Electrolytes: Validity of Common Electrochemical Stability Window (ESW) Data and Alternative Strategies. *Phys. Chem. Chem. Phys.* **2017**, *19*, 16078–16086.
(38) Xiao, X.; Liu, Z.; Baggetto, L.; Veith, G. M.; More, K. L.; Unocic, R. R. Unraveling Manganese Dissolution/Deposition Mechanisms on the Negative Electrode in Lithium Ion Batteries. *Phys. Chem. Chem. Phys.* **2014**, *16* (22), 10398–10402.
(39) Gowda, S. R.; Gallagher, K. G.; Croy, J. R.; Bettge, M.; Thackeray, M. M.; Balasubramanian, M. Oxidation State of Cross-over Manganese Species on the Graphite Electrode of Lithium-Ion Cells. *Phys. Chem. Chem. Phys.* **2014**, *16* (15), 6898–6902.
(40) Nordh, T.; Younesi, R.; Hahlin, M.; Duarte, R. F.; Tengstedt, C.; Brandell, D.; Edström, K. Manganese in the SEI Layer of Li4Ti5O12 Studied by Combined NEXAFS and HAXPES Techniques. *J. Phys. Chem. C* **2016**, *120* (6), 3206–3213.
(41) Zhan, C.; Lu, J.; Kropf, A. J.; Wu, T.; Jansen, A. N.; Sun, Y.-K.; Qiu, X.; Amine, K. Mn(II) Deposition on Anodes and Its Effects on Capacity Fade in Spinel Lithium Manganate-Carbon Systems. *Nat. Commun.* **2013**, *4*, 2437.
(42) Tang, D.; Ben, L.; Sun, Y.; Chen, B.; Yang, Z.; Gu, L.; Huang, X. Electrochemical Behavior and Surface Structural Change of LiMn 2 O 4 Charged to 5.1 V. *J. Mater. Chem. A* **2014**, *2*, 14519.
(43) Gallus, D. R.; Schmitz, R.; Wagner, R.; Hoffmann, B.; Nowak, S.; Cekic-Laskovic, I.; Schmitz, R. W.; Winter, M. The Influence of Different Conducting Salts on the Metal Dissolution and Capacity Fading of NCM Cathode Material. *Electrochim. Acta* **2014**, *134*, 393–398.
(44) Lu, J.; Zhan, C.; Wu, T.; Wen, J.; Lei, Y.; Kropf, A. J.; Wu, H.; Miller, D. J.; Elam, J. W.; Sun, Y.-K.; Qiu, X.; Amine, K. Effectively Suppressing Dissolution of Manganese from Spinel Lithium Manganate via a Nanoscale Surface-Doping Approach. *Nat. Commun.* **2014**, *5* (May), 5693.
(45) Birkenmaier, C.; Bitzer, B.; Harzheim, M.; Hintennach, A.; Schleid, T. Lithium Plating on Graphite Negative Electrodes: Innovative Qualitative and Quantitative Investigation Methods. *J. Electrochem. Soc.* **2015**, *162* (14), A2646–A2650.

(46) Petzl, M.; Danzer, M. A. Nondestructive Detection, Characterization, and Quantification of Lithium Plating in Commercial Lithium-Ion Batteries. *J. Power Sources* **2014**, *254*, 80–87.
(47) An, S. J.; Li, J.; Daniel, C.; Mohanty, D.; Nagpure, S.; Wood, D. L. The State of Understanding of the Lithium-Ion-Battery Graphite Solid Electrolyte Interphase (SEI) and Its Relationship to Formation Cycling. *Carbon N. Y.* **2016**, *105*, 52–76.
(48) Shen, C.; Hu, G.; Cheong, L.-Z.; Huang, S.; Zhang, J.-G.; Wang, D. Direct Observation of the Growth of Lithium Dendrites on Graphite Anodes by Operando EC-AFM. *Small Methods* **2017**, *2* (2), 1700298.
(49) Su, X.; Dogan, F.; Ilavsky, J.; Maroni, V. A.; Gosztola, D. J.; Lu, W. Mechanisms for Lithium Nucleation and Dendrite Growth in Selected Carbon Allotropes. *Chem. Mater.* **2017**, *29* (15), 6205–6213.
(50) Spahr, M. E.; Palladino, T.; Wilhelm, H.; Würsig, A.; Goers, D.; Buqa, H.; Holzapfel, M.; Novák, P. Exfoliation of Graphite during Electrochemical Lithium Insertion in Ethylene Carbonate-Containing Electrolytes. *J. Electrochem. Soc.* **2004**, *151* (9), A1383.
(51) Aurbach, D.; Ein-Eli, Y. The Study of Li-Graphite Intercalation Processes in Several Electrolyte Systems Using In Situ X-Ray Diffraction. *J. Electrochem. Soc.* **1995**, *142* (6), 1746–1752.
(52) Lin, F.; Markus, I. M.; Nordlund, D.; Weng, T.-C.; Asta, M. D.; Xin, H. L.; Doeff, M. M. Surface Reconstruction and Chemical Evolution of Stoichiometric Layered Cathode Materials for Lithium-Ion Batteries. *Nat. Commun.* **2014**, *5*, 3529.
(53) Höweling, A.; Glatthaar, S.; Nötzel, D.; Binder, J. R. Evidence of Loss of Active Lithium in Titanium-Doped LiNi 0.5 Mn 1.5 O 4 /Graphite Cells. *J. Power Sources* **2014**, *274*, 1267–1275.
(54) Holtstiege, F.; Wilken, A.; Winter, M.; Placke, T. Running out of Lithium? A Route to Differentiate between Capacity Losses and Active Lithium Losses in Lithium-Ion Batteries. *Phys. Chem. Chem. Phys.* **2017**, *19* (38), 25905–25918.
(55) Chen, Z.; Wang, J.; Chao, D.; Baikie, T.; Bai, L.; Chen, S.; Zhao, Y.; Sum, T. C.; Lin, J.; Shen, Z. Hierarchical Porous LiNi 1/3 Co 1/3 Mn 1/3 O 2 Nano-/Micro Spherical Cathode Material: Minimized Cation Mixing and Improved Li + Mobility for Enhanced Electrochemical Performance. *Sci. Rep.* **2016**, *6* (April), 1–10.
(56) Guo, S.; Sun, Y.; Liu, P.; Yi, J.; He, P.; Zhang, X.; Zhu, Y.; Senga, R.; Suenaga, K.; Chen, M.; Zhou, H. Cation-Mixing Stabilized Layered Oxide Cathodes for Sodium-Ion Batteries. *Sci. Bull.* **2018**, *63* (6), 376–384.
(57) Abdellahi, A.; Urban, A.; Dacek, S.; Ceder, G. Understanding the Effect of Cation Disorder on the Voltage Profile of Lithium Transition-Metal Oxides. *Chem. Mater.* **2016**, *28* (15), 5373–5383.
(58) Zheng, S.; Huang, R.; Makimura, Y.; Ukyo, Y.; Fisher, C. A. J.; Hirayama, T.; Ikuhara, Y. Microstructural Changes in LiNi0.8Co0.15Al0.05O2 Positive Electrode Material during the First Cycle. *J. Electrochem. Soc.* **2011**, *158* (4), A357.
(59) Yoon, T.; Park, S.; Mun, J.; Ryu, J. H.; Choi, W.; Kang, Y. S.; Park, J. H.; Oh, S. M. Failure Mechanisms of LiNi 0.5Mn 1.5O 4 Electrode at Elevated Temperature. *J. Power Sources* **2012**, *215*, 312–316.
(60) Fransson, L.; Eriksson, T.; Edström, K.; Gustafsson, T.; Thomas, J. O. Influence of Carbon Black and Binder on Li-Ion Batteries. *J. Power Sources* **2001**, *101* (1), 1–9.

(61) Lux, S. F.; Chevalier, J.; Lucas, I. T.; Kostecki, R. HF Formation in LiPF6-Based Organic Carbonate Electrolytes. *ECS Electrochem. Lett.* **2013**, *2* (12), A121–A123.
(62) Rozier, P.; Tarascon, J. M. Review—Li-Rich Layered Oxide Cathodes for Next-Generation Li-Ion Batteries: Chances and Challenges. *J. Electrochem. Soc.* **2015**, *162* (14), A2490–A2499.
(63) Berg, E. J.; Villevieille, C.; Streich, D.; Trabesinger, S.; Novák, P. Rechargeable Batteries: Grasping for the Limits of Chemistry. *J. Electrochem. Soc.* **2015**, *162* (14), A2468–A2475.
(64) Kim, J. W.; Travis, J. J.; Hu, E.; Nam, K. W.; Kim, S. C.; Kang, C. S.; Woo, J. H.; Yang, X. Q.; George, S. M.; Oh, K. H.; Cho, S. J.; Lee, S. H. Unexpected High Power Performance of Atomic Layer Deposition Coated Li[Ni1/3Mn1/3Co1/3]O2 Cathodes. *J. Power Sources* **2014**, *254*, 190–197.
(65) Nayak, P. K.; Grinblat, J.; Levi, M.; Wu, Y.; Powell, B.; Aurbach, D. TEM and Raman Spectroscopy Evidence of Layered to Spinel Phase Transformation in Layered LiNi1/3Mn1/3Co1/3O2 upon Cycling to Higher Voltages. *J. Electroanal. Chem.* **2014**, *733*, 6–19.
(66) Liu, H.; Bugnet, M.; Tessaro, M. Z.; Harris, K. J.; Dunham, M. J. R.; Jiang, M.; Goward, G. R.; Botton, G. A. Spatially Resolved Surface Valence Gradient and Structural Transformation of Lithium Transition Metal Oxides in Lithium-Ion Batteries. *Phys. Chem. Chem. Phys.* **2016**, *18* (42), 29064–29075.
(67) Buchberger, I.; Seidlmayer, S.; Pokharel, A.; Piana, M.; Hattendorff, J.; Kudejova, P.; Gilles, R.; Gasteiger, H. A. Aging Analysis of Graphite/LiNi1/3Mn1/3Co1/3O2 Cells Using XRD, PGAA, and AC Impedance. *J. Electrochem. Soc.* **2015**, *162* (14), A2737–A2746.
(68) Joshi, T.; Eom, K.; Yushin, G.; Fuller, T. F. Effects of Dissolved Transition Metals on the Electrochemical Performance and SEI Growth in Lithium-Ion Batteries. *J. Electrochem. Soc.* **2014**, *161* (12), A1915–A1921.
(69) Smith, A. J.; Smith, S. R.; Byrne, T.; Burns, J. C.; Dahn, J. R. Synergies in Blended LiMn2O4 and Li[Ni1/3Mn1/3Co1/3]O2 Positive Electrodes. *J. Electrochem. Soc.* **2012**, *159* (10), A1696–A1701.
(70) Kızıltaş-Yavuz, N.; Herklotz, M.; Hashem, A. M.; Abuzeid, H. M.; Schwarz, B.; Ehrenberg, H.; Mauger, A.; Julien, C. M. Synthesis, Structural, Magnetic and Electrochemical Properties of LiNi1/3Mn1/3Co1/3O2 Prepared by a Sol–gel Method Using Table Sugar as Chelating Agent. *Electrochim. Acta* **2013**, *113*, 313–321.
(71) Schipper, F.; Erickson, E. M.; Erk, C.; Shin, J.-Y.; Chesneau, F. F.; Aurbach, D. Review—Recent Advances and Remaining Challenges for Lithium Ion Battery Cathodes. *J. Electrochem. Soc.* **2017**, *164* (1), A6220–A6228.
(72) Mohanty, D.; Dahlberg, K.; King, D. M.; David, L. A.; Sefat, A. S.; Wood, D. L.; Daniel, C.; Dhar, S.; Mahajan, V.; Lee, M.; Albano, F. Modification of Ni-Rich FCG NMC and NCA Cathodes by Atomic Layer Deposition: Preventing Surface Phase Transitions for High-Voltage Lithium-Ion Batteries. *Sci. Rep.* **2016**, *6* (February), 26532.
(73) Sun, Y. K.; Myung, S. T.; Kim, M. H.; Prakash, J.; Amine, K. Synthesis and Characterization of Li[(Ni0.8Co 0.1Mn0.1)0.8(Ni0.5Mn 0.5)0.2]O2 with the Microscale Core-Shell Structure as the Positive Electrode Material for Lithium Batteries. *J. Am. Chem. Soc.* **2005**, *127* (38), 13411–13418.
(74) Yoon, C. S.; Park, K. J.; Kim, U. H.; Kang, K. H.; Ryu, H. H.; Sun, Y. K. High-Energy Ni-Rich Li[NixCoyMn1-x-y]O2Cathodes via Compositional Partitioning for Next-Generation Electric Vehicles. *Chem. Mater.* **2017**, *29* (24), 10436–10445.

(75) Axnanda, S.; Crumlin, E. J.; Mao, B.; Rani, S.; Chang, R.; Karlsson, P. G.; Edwards, M. O. M.; Lundqvist, M.; Moberg, R.; Ross, P.; Hussain, Z.; Liu, Z. Using "Tender" X-Ray Ambient Pressure X-Ray Photoelectron Spectroscopy as A Direct Probe of Solid-Liquid Interface. *Sci. Rep.* **2015**, *5* (October 2014), 9788.

(76) Fadley, C. S. X-Ray Photoelectron Spectroscopy: Progress and Perspectives. *J. Electron Spectros. Relat. Phenomena* **2010**, *178–179* (C), 2–32.

(77) Bagus, P. S.; Ilton, E. S.; Nelin, C. J. The Interpretation of XPS Spectra: Insights into Materials Properties. *Surf. Sci. Rep.* **2013**, *68* (2), 273–304.

(78) Kerber, S. J.; Barr, T. L.; Mann, G. P.; Brantley, W. A.; Papazoglou, E.; Mitchell, J. C. The Complementary Nature of X-Ray Photoelectron Spectroscopy and Angle-Resolved X-Ray Diffraction Part I : Background and Theory. *J. Mater. Eng. Perform.* **1998**, *7* (June), 329–333.

(79) Bodenes, L.; Dedryvere, R.; Martinez, H.; Fischer, F.; Tessier, C.; Peres, J.-P. Lithium-Ion Batteries Working at 85 C: Aging Phenomena and Electrode/Electrolyte Interfaces Studied by XPS. *J. Electrochem. Soc.* **2012**, *159* (10), A1739–A1746.

(80) Crist, B. V. A Review of XPS Data-Banks. *J. AES XPS Reports* **2007**, *39*, 1–53.

(81) Wagner, C. D.; Davis, L. E.; Zeller, M. V; Taylor, J. A.; Raymond, R. H.; Gale, L. H. Empirical Atomic Sensitivity Factors for Quantitative Analysis by Electron Spectroscopy for Chemical Analysis. *Surf. Interface Anal.* **1981**, *3* (5), 211–225.

(82) Moulder, J. F.; Stickle, W. F.; Sobol, P. E.; Bomben, K. D. *Handbook of X-Ray Photoelectron Spectroscopy*; Chastain, J., King, R. C., Eds.; Physical Electronics, Inc.: Eden Prairie, 1995.

(83) Smith, G. C. Evaluation of a Simple Correction for the Hydrocarbon Contamination Layer in Quantitative Surface Analysis by XPS. *J. Electron Spectros. Relat. Phenomena* **2005**, *148* (1), 21–28.

(84) Ciosek Högström, K.; Malmgren, S.; Hahlin, M.; Gorgoi, M.; Nyholm, L.; Rensmo, H.; Edström, K. The Buried Carbon/Solid Electrolyte Interphase in Li-Ion Batteries Studied by Hard x-Ray Photoelectron Spectroscopy. *Electrochim. Acta* **2014**, *138*, 430–436.

(85) Philippe, B.; Hahlin, M.; Edström, K.; Gustafsson, T.; Siegbahn, H.; Rensmo, H. Photoelectron Spectroscopy for Lithium Battery Interface Studies. *J. Electrochem. Soc.* **2016**, *163* (2), A178–A191.

(86) Fernández-García, M. XANES Analysis of Catalytic Systems under Reaction Conditions. *Catal. Rev. Sci. Eng.* **2002**, *44* (1), 59–121.

(87) Gaur, A.; Shrivastava, B. D.; Nigam, H. L. X-Ray Absorption Fine Structure (XAFS) Spectroscopy – A Review. *Proc Indian Natn Sci Acad Spl. Issue, Part B* **2013**, *79* (4), 921–966.

(88) Szabo, F. K.; Hoffman, G. E. NIH Public Access. **2012**, *37* (1), 62–70.

(89) Henderson, G. S.; Groot, F. M. F. De; Moulton, B. J. A. X-Ray Absorption Near-Edge Structure (XANES) Spectroscopy. **2014**, *78*, 75–138.

(90) Yano, J.; Yachandra, V. K. X-Ray Absorption Spectroscopy. *Photosynth. Res.* **2009**, *102* (2), 241–254.

(91) Dai, Y.; Gorey, T. J.; Anderson, S. L.; Lee, S.; Lee, S.; Seifert, S.; Winans, R. E. Inherent Size Effects on XANES of Nanometer Metal Clusters: Size-Selected Platinum Clusters on Silica. *J. Phys. Chem. C* **2017**, *121* (1), 361–374.

(92) Sham, T. K. Nanoparticles and Nanowires: Synchrotron Spectroscopy Studies. *Int. J. Nanotechnol.* **2008**, *5*, 1194.

(93) Wong, J. O. E. Extended X-Ray Absorption F i n e Structure : A Modern Structural Tool in Materials Science. *Mater. Sci. Eng.* **1986**, *80*, 107–128.
(94) Penner-Hahn, J. E. X-Ray Absorption Spectroscopy in Coordination Chemistry. *Coord. Chem. Rev.* **1999**, *190–192*, 1101–1123.
(95) Davoli, I.; Paris, E.; Mottana, A.; Marcelli, A. Xanes Analysis on Pyroxenes with Different ca Concentration in M2 Site. *Phys. Chem. Miner.* **1987**, *14* (1), 21–25.
(96) Yamamoto, T. Assignment of Pre-Edge Peaks in K-Edge x-Ray Absorption Spectra of 3d Transition Metal Compounds: Electric Dipole or Quadrupole? *X-Ray Spectrom.* **2008**, *37*, 572–584.
(97) Yoon, W.-S.; Paik, Y.; Yang, X.-Q.; Balasubramanian, M.; McBreen, J.; Grey, C. P. Investigation of the Local Structure of the LiNi0.5Mn0.5O2 Cathode Material during Electrochemical Cycling by X-Ray Absorption and NMR Spectroscopy. *Electrochem. Solid-State Lett.* **2002**, *5* (11), A263.
(98) Koyama, Y.; Yabuuchi, N.; Tanaka, I.; Adachi, H.; Ohzuku, T. Solid-State Chemistry and Electrochemistry of LiCo1/3Ni1/3Mn1/3O2 for Advanced Lithium-Ion Batteries. *J. Electrochem. Soc.* **2004**, *151* (10), A1545.
(99) Yabuuchi, N.; Makimura, Y.; Ohzuku, T. Solid-State Chemistry and Electrochemistry of LiCo[Sub 1⁄3]Ni[Sub 1⁄3]Mn[Sub 1⁄3]O[Sub 2] for Advanced Lithium-Ion Batteries. *J. Electrochem. Soc.* **2007**, *154* (4), A314–A321.
(100) Xu, C.; Jeschull, F.; Brant, W. R.; Brandell, D.; Edström, K.; Gustafsson, T. The Role of LiTDI Additive in $LiNi_{1/3}Mn_{1/3}Co_{1/3}O_2$ /Graphite Lithium-Ion Batteries at Elevated Temperatures. *J. Electrochem. Soc.* **2018**, *165* (2), A40–A46.
(101) Liu, X.; Wang, D.; Liu, G.; Srinivasan, V.; Liu, Z.; Hussain, Z.; Yang, W. Distinct Charge Dynamics in Battery Electrodes Revealed by in Situ and Operando Soft X-Ray Spectroscopy. *Nat. Commun.* **2013**, *4* (May), 1–8.
(102) Cherkashinin, G.; Motzko, M.; Schulz, N.; Späth, T.; Jaegermann, W. Electron Spectroscopy Study of Li[Ni,Co,Mn]O<inf>2</Inf>/Electrolyte Interface: Electronic Structure, Interface Composition, and Device Implications. *Chem. Mater.* **2015**, *27* (8), 2875–2887.
(103) Lindgren, F.; Xu, C.; Niedzicki, L.; Marcinek, M.; Gustafsson, T.; Björefors, F.; Edström, K.; Younesi, R. SEI Formation and Interfacial Stability of a Si Electrode in a LiTDI-Salt Based Electrolyte with FEC and VC Additives for Li-Ion Batteries. *ACS Appl. Mater. Interfaces* **2016**, *8* (24), 15758–15766.
(104) Xia, J.; Petibon, R.; Xiong, D.; Ma, L.; Dahn, J. R. Enabling Linear Alkyl Carbonate Electrolytes for High Voltage Li-Ion Cells. *J. Power Sources* **2016**, *328*, 124–135.
(105) Aktekin, B.; Lacey, M. J.; Nordh, T.; Younesi, R.; Tengstedt, C.; Zipprich, W.; Brandell, D.; Edström, K. Understanding the Capacity Loss in LiNi0.5Mn1.5O4-Li4Ti5O12Lithium-Ion Cells at Ambient and Elevated Temperatures. *J. Phys. Chem. C* **2018**, *122* (21), 11234–11248.
(106) Philippe, B.; Dedryveère, R.; Gorgoi, M.; Rensmo, H.; Gonbeau, D.; Edström, K. Role of the LiPF6 Salt for the Long-Term Stability of Silicon Electrodes in Li-Ion Batteries - A Photoelectron Spectroscopy Study. *Chem. Mater.* **2013**, *25* (3), 394–404.
(107) Xing, L.; Vatamanu, J.; Borodin, O.; Smith, G. D.; Bedrov, D. Electrode/Electrolyte Interface in Sulfolane-Based Electrolytes for Li Ion Batteries: A Molecular Dynamics Simulation Study. *J. Phys. Chem. C* **2012**, *116* (45), 23871–23881.

(108) Tebbe, J. L.; Holder, A. M.; Musgrave, C. B. Mechanisms of LiCoO2 Cathode Degradation by Reaction with HF and Protection by Thin Oxide Coatings. *ACS Appl. Mater. Interfaces* **2015**, *7* (43), 24265–24278.
(109) Heider, U.; Oesten, R.; Jungnitz, M. Challenge in Manufacturing Electrolyte Solutions for Lithium and Lithium Ion Batteries Quality Control and Minimizing Contamination Level. *J. Power Sources* **1999**, *81–82*, 119–122.

Acta Universitatis Upsaliensis

Digital Comprehensive Summaries of Uppsala Dissertations from the Faculty of Science and Technology 1802

Editor: The Dean of the Faculty of Science and Technology

A doctoral dissertation from the Faculty of Science and Technology, Uppsala University, is usually a summary of a number of papers. A few copies of the complete dissertation are kept at major Swedish research libraries, while the summary alone is distributed internationally through the series Digital Comprehensive Summaries of Uppsala Dissertations from the Faculty of Science and Technology. (Prior to January, 2005, the series was published under the title "Comprehensive Summaries of Uppsala Dissertations from the Faculty of Science and Technology".)

Distribution: publications.uu.se
urn:nbn:se:uu:diva-381548

ACTA
UNIVERSITATIS
UPSALIENSIS
UPPSALA
2019